NAVAL POSTGRADUATE SCHOOL

MONTEREY, CALIFORNIA

THESIS

IMPACT OF UNDERWATER EXPLOSIONS ON CONCRETE BRIDGE FOUNDATIONS

by

Jean B. Loomis

June 2016

Thesis Advisor: Jarema M. Didoszak
Co-Advisor: Young W. Kwon

THIS PAGE INTENTIONALLY LEFT BLANK

REPORT DOCUMENTATION PAGE			Form Approved OMB No. 0704–0188
Public reporting burden for this collection of information is estimated to average 1 hour per response, including the time for reviewing instruction, searching existing data sources, gathering and maintaining the data needed, and completing and reviewing the collection of information. Send comments regarding this burden estimate or any other aspect of this collection of information, including suggestions for reducing this burden, to Washington headquarters Services, Directorate for Information Operations and Reports, 1215 Jefferson Davis Highway, Suite 1204, Arlington, VA 22202-4302, and to the Office of Management and Budget, Paperwork Reduction Project (0704-0188) Washington, DC 20503.			
1. AGENCY USE ONLY ***(Leave blank)***	**2. REPORT DATE** June 2016	**3. REPORT TYPE AND DATES COVERED** Master's thesis	
4. TITLE AND SUBTITLE IMPACT OF UNDERWATER EXPLOSIONS ON CONCRETE BRIDGE FOUNDATIONS		**5. FUNDING NUMBERS**	
6. AUTHOR(S) Jean B. Loomis			
7. PERFORMING ORGANIZATION NAME(S) AND ADDRESS(ES) Naval Postgraduate School Monterey, CA 93943-5000		**8. PERFORMING ORGANIZATION REPORT NUMBER**	
9. SPONSORING /MONITORING AGENCY NAME(S) AND ADDRESS(ES) N/A		**10. SPONSORING / MONITORING AGENCY REPORT NUMBER**	
11. SUPPLEMENTARY NOTES The views expressed in this thesis are those of the author and do not reflect the official policy or position of the Department of Defense or the U.S. Government. IRB Protocol number ____N/A____.			
12a. DISTRIBUTION / AVAILABILITY STATEMENT Approved for public release; distribution is unlimited		**12b. DISTRIBUTION CODE**	

13. ABSTRACT (maximum 200 words)

In the event an underwater improvised explosive device (IED) were placed near a bridge, Explosive Ordinance Disposal (EOD) units would typically mitigate the threat by conducting a controlled detonation of the bomb. The controlled detonation must be executed a safe distance from any critical infrastructure to ensure the survivability of the structure. This thesis implements the Dynamic System Mechanics Advanced Simulation to characterize a safe detonation distance by determining the critical scenario contributing toward bridge failure. Efforts were also made to determine the parameters critical to modeling bridge foundations.

To characterize the most critical scenario, trinitrotoluene was detonated at varying horizontal standoff distances and at varying water depths. The interaction of the underwater explosion (UNDEX) with a bridge foundation modeled from an actual bridge was observed. Intermediate depths were the most damaging to the foundation when the bomb was detonated near the surface of the water and when the bomb was located at the sand-water interface. Subsequently, EOD units should aim for controlled detonations in shallow or deep water.

Two parameters, load and rebar reinforcement volume fraction, were varied to observe their impact on the foundation's response to an UNDEX. The damage to the foundation was minimal as the load fluctuated, indicating that these loads do not need to be properly modeled. When the reinforcement was placed entirely in the X-, Y-, or Z-dimension, the rebar perpendicular to the shockwave proved to be the most critical. Changes in reinforcement volume fraction are also not important in short simulations. As the simulation is extended, the dependence of the damage on the volume fraction increases. As such, foundation models do not need to accurately model the load, but must properly model the reinforcement perpendicular to the shockwave and the volume fraction, if the simulation is long. Understanding which foundational components are critical to its survivability allow bridge foundations to be grouped based on these components, such as reinforcement volume fraction.

14. SUBJECT TERMS UNDEX, DYSMAS, DYNA, Gemini, infrastructure, bridge, Eulerian, Lagrangian			**15. NUMBER OF PAGES** 99
			16. PRICE CODE
17. SECURITY CLASSIFICATION OF REPORT Unclassified	**18. SECURITY CLASSIFICATION OF THIS PAGE** Unclassified	**19. SECURITY CLASSIFICATION OF ABSTRACT** Unclassified	**20. LIMITATION OF ABSTRACT** UU

NSN 7540–01-280-5500 Standard Form 298 (Rev. 2–89)
Prescribed by ANSI Std. 239–18

THIS PAGE INTENTIONALLY LEFT BLANK

Approved for public release; distribution is unlimited

IMPACT OF UNDERWATER EXPLOSIONS ON CONCRETE BRIDGE FOUNDATIONS

Jean B. Loomis
Ensign, United States Navy
B.S., United States Naval Academy, 2015

Submitted in partial fulfillment of the
requirements for the degree of

MASTER OF SCIENCE IN MECHANICAL ENGINEERING

from the

NAVAL POSTGRADUATE SCHOOL
June 2016

Approved by: Jarema M. Didoszak
Thesis Advisor

Young W. Kwon, Ph.D.
Co-Advisor

Garth V. Hobson, Ph.D.
Chair, Department of Mechanical and Aerospace Engineering

THIS PAGE INTENTIONALLY LEFT BLANK

ABSTRACT

In the event an underwater improvised explosive device (IED) were placed near a bridge, Explosive Ordinance Disposal (EOD) units would typically mitigate the threat by conducting a controlled detonation of the bomb. The controlled detonation must be executed a safe distance from any critical infrastructure to ensure the survivability of the structure. This thesis implements the Dynamic System Mechanics Advanced Simulation to characterize a safe detonation distance by determining the critical scenario contributing toward bridge failure. Efforts were also made to determine the parameters critical to modeling bridge foundations.

To characterize the most critical scenario, trinitrotoluene was detonated at varying horizontal standoff distances and at varying water depths. The interaction of the underwater explosion (UNDEX) with a bridge foundation modeled from an actual bridge was observed. Intermediate depths were the most damaging to the foundation when the bomb was detonated near the surface of the water and when the bomb was located at the sand-water interface. Subsequently, EOD units should aim for controlled detonations in shallow or deep water.

Two parameters, load and rebar reinforcement volume fraction, were varied to observe their impact on the foundation's response to an UNDEX. The damage to the foundation was minimal as the load fluctuated, indicating that these loads do not need to be properly modeled. When the reinforcement was placed entirely in the X-, Y-, or Z-dimension, the rebar perpendicular to the shockwave proved to be the most critical. Changes in reinforcement volume fraction are also not important in short simulations. As the simulation is extended, the dependence of the damage on the volume fraction increases. As such, foundation models do not need to accurately model the load but must properly model the reinforcement perpendicular to the shockwave and the volume fraction if the simulation is long. Understanding which foundational components are critical to their survivability allow bridge foundations to be grouped based on these components, such as reinforcement volume fraction.

THIS PAGE INTENTIONALLY LEFT BLANK

TABLE OF CONTENTS

LIST OF FIGURES

THIS PAGE INTENTIONALLY LEFT BLANK

LIST OF TABLES

THIS PAGE INTENTIONALLY LEFT BLANK

ACKNOWLEDGMENTS

I would first and foremost like to thank the entire faculty at the Naval Postgraduate School for this opportunity and their support. I would like to especially thank my research advisor, Professor Jarema Didoszak, for endlessly helping me navigate the seemingly foreign languages of DYSMAS, DYNA, and Gemini. My co-advisor, Dr. Young Kwon, also provided immeasurable guidance in both life and with my thesis research.. I will be forever grateful for his patience and persistence. Finally, I would like to extend a special thank you to Mr. Frank Fiumano and the United States Coast Guard Station of Staten Island as well as the port partners of New York City—to include the Metropolitan Transit Authority and New York Police Department Harbor Unit and Scuba Team—for their fantastic tour of the Hudson River.

THIS PAGE INTENTIONALLY LEFT BLANK

I. INTRODUCTION

A. BACKGROUND

Bridges are a vital component of modern life. Because bridges are such a critical infrastructure, they need to be completely functional as often as possible. Standard maintenance is an unavoidable obstruction in a bridge's lifetime; however, any unplanned interferences must be neutralized as efficiently as possible. Mines and IEDs represent one of the greatest threats to the functionality of a bridge. The standard method in dealing with an ordinance is to explode the ordinance in a controlled environment while ensuring that minimal damage is done to any assets. It is therefore vital to know the safe distance that an explosive of a given size can be detonated from a bridge.

Conducting full-scale tests on bridges using underwater explosives is not practical; therefore, this problem must be addressed through modeling. Recent developments in modeling software have allowed detailed simulations to be generated using the Dynamic System Mechanics Advanced Simulation (DYSMAS) suite [1]. DYSMAS is a three dimensional finite element code designed to study the effects of an explosive charge on a user-defined structure. DYSMAS uses Eulerian fluid equations to conduct a finite element analysis of the water during an underwater explosion (UNDEX). Lagrangian finite element equations of motion study the movement of the structure. Essentially, the user picks a section of the water surrounding the structure and examines the flow of the water throughout this section, which is an Eulerian analysis. The user also studies the motion of each particle as it moves throughout the structure, a Lagrangian analysis. The program combines the Eulerian and Lagrangian methods to develop a fully coupled system.

Previous research has used DYSMAS to study the impact of UNDEX on pipelines and tunnels; however, there has been no thorough investigation on the impact of underwater explosions on major highway bridge pilings. The use of concrete in pilings poses one of the greatest obstructions to proper modeling because of crack propagation that is the signature of concrete failure. That being said, DYSMAS can implement

DYNA3D Material Type 66 to captures the slow failure of concrete while also modeling the rebar reinforcement of the pilings. Employing DYSMAS and structural knowledge of a critical bridge, the results of this research will allow operational commanders to anticipate the effects of underwater explosions on nearby infrastructure. This knowledge will be critical in making effective decisions during mine countermeasure operations.

B. SCOPE OF RESEARCH

Bridge survivability is a concern for the economy and safety of multiple major cities. Understanding the impact of an explosion on the functionality of a bridge will help EOD units neutralize bomb threats near these bridges. This thesis will implement DYSMAS to execute a series of studies that will allow unit commanders to understand factors impacting the safe distance to detonate a bomb of a given size. There will also be a brief study on the impact of water depth on the damage to the foundation.

A series of parametric studies will also be conducted to explore the sensitivity of the foundation to changes in loading conditions and configurations in rebar reinforcement. The goal of these studies is to determine how accurate the model needs to be in order to produce comparable results. These studies are important for older infrastructure where there is minimal documentation on the construction. Modeling efforts therefore require estimation. These studies will determine how accurate the estimation must be to generate meaningful results.

II. UNDERWATER SHOCK EXPLOSION THEORY

There are three primary phases to an underwater explosion (UNDEX): the detonation, formation of the shock wave, and bulk cavitation. Depending on various circumstances, such as the depth of the water and hardness of the sediment, the UNDEX can produce surface effects as seen in Figure 1. Additionally, dynamic loading will be placed on any structures close to the event, such as a bridge piling. This section will delineate a fundamental knowledge of UNDEX to be applied in the development of the DYSMAS model.

Figure 1. Underwater explosion observed from the surface. Source: [2].

The explosion of an UNDEX is an exothermic chemical reaction that continues to propagate after the initial event. This reaction generates temperatures of 3000 degrees Celsius and pressures of 50000 atmospheres [3]. DYSMAS can model a wide variety of

explosives, but this study will focus on trinitrotoluene (TNT), the most common explosive. TNT is composed of $C_7H_5N_3O_6$, has a density of 1600 kg/m^3 (99.9 pcf), and moves 6940 m/s (22769 ft. /s) upon detonation.

After detonation, a shock wave is created and expands rapidly away from the source of the explosion. Outside of 2–3 radii of the charge, the propagation of the shock wave is linear. Trapped inside a high-pressure sphere within the shock wave are the remaining gases [2]. These gases will fight to expand to achieve equilibrium with the hydrostatic pressure around it, but it will lose a great deal of energy through the growth. As a result, the gas bubble will contract, which will again cause an increase in pressure and a subsequent growth of the bubble. The bubble will continue to expand and contract until its energy is drained. Due to Archimedes principle, the bubble will rise to the surface of the water as it shrinks. Figure 2 shows a cross section of the bubble growth and what the pulse would look like from the surface.

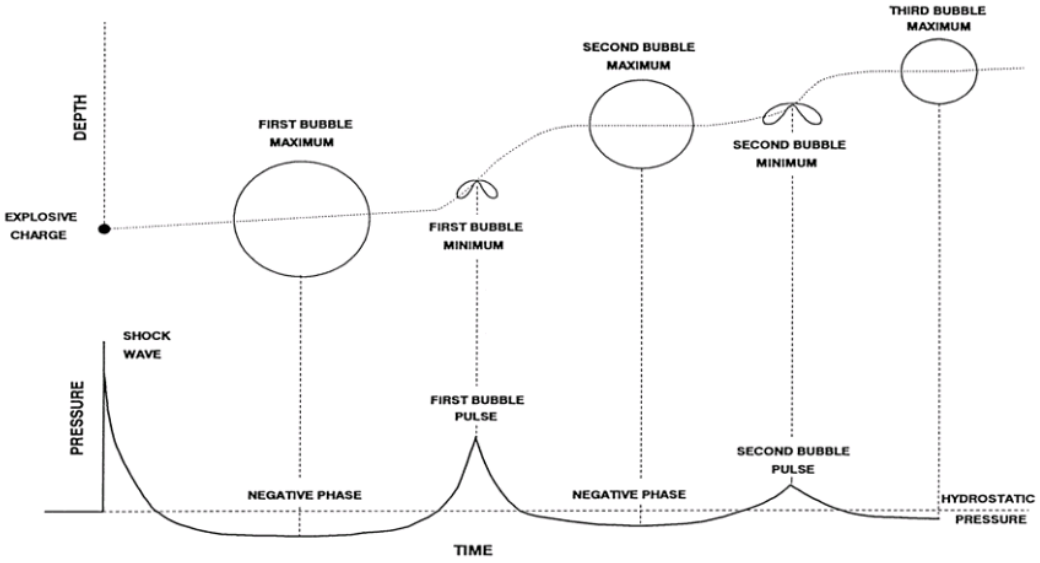

Figure 2. Bubble pulsing to the surface. Source: [3].

A portion of the shock wave that travels to the surface is reflected back from the surface and creates a region known as the cavitated layer. The surface reflects a tensile wave into the fluid, creating a vaporous region just below the surface of the water. This region only exists for a few milliseconds because it is rapidly closed due to gravity and

the atmospheric pressure acting on the thin layer of water above it. When the layer is snapped shut, the upper layer of water crashes onto the lower layer, generating a secondary shock wave known as a bulk cavitation closure pulse [4]. Figure 3 shows a cavitation layer and chart of the various loading over time. It is worth noting that the cavitation pulse is somewhat exaggerated and will not be as large in practice.

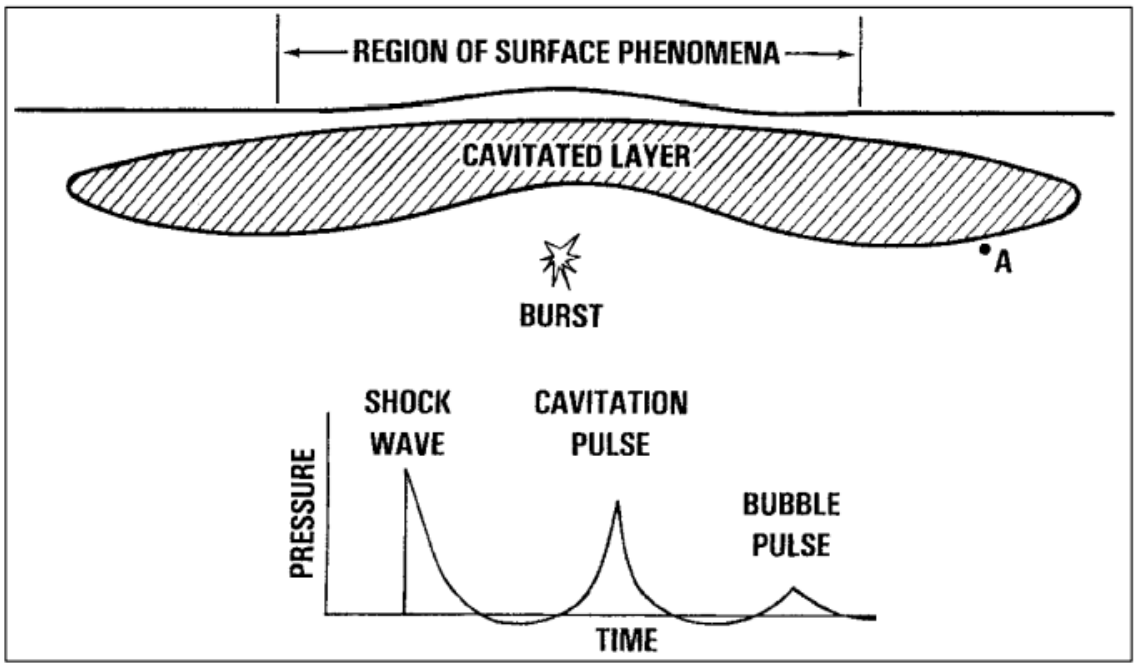

Figure 3. Bulk cavitation at the surface and pressure history over the course of an UNDEX. Source: [2].

Reflection of the shock wave off the surface and bottom sediment will greatly increase the dynamic loading placed on a structure. Thermal gradients in the water will break down any linear assumptions made about incident shock waves; therefore, any modeling will assume a water of constant temperature. For shock waves that reflect directly from the bottom or surface, Snell's law will govern the reflection. In practice some energy will be absorbed by the bottom sediment, however, the modeling will take a conservative approach and assume that all of the shock energy will be reflected off the bottom of the waterway. Because all energy is assumed to be reflected, waves that may

travel partially through the bottom material will be neglected. Figure 4 pulls together all of the major components of an UNDEX and shows how they relate to each other.

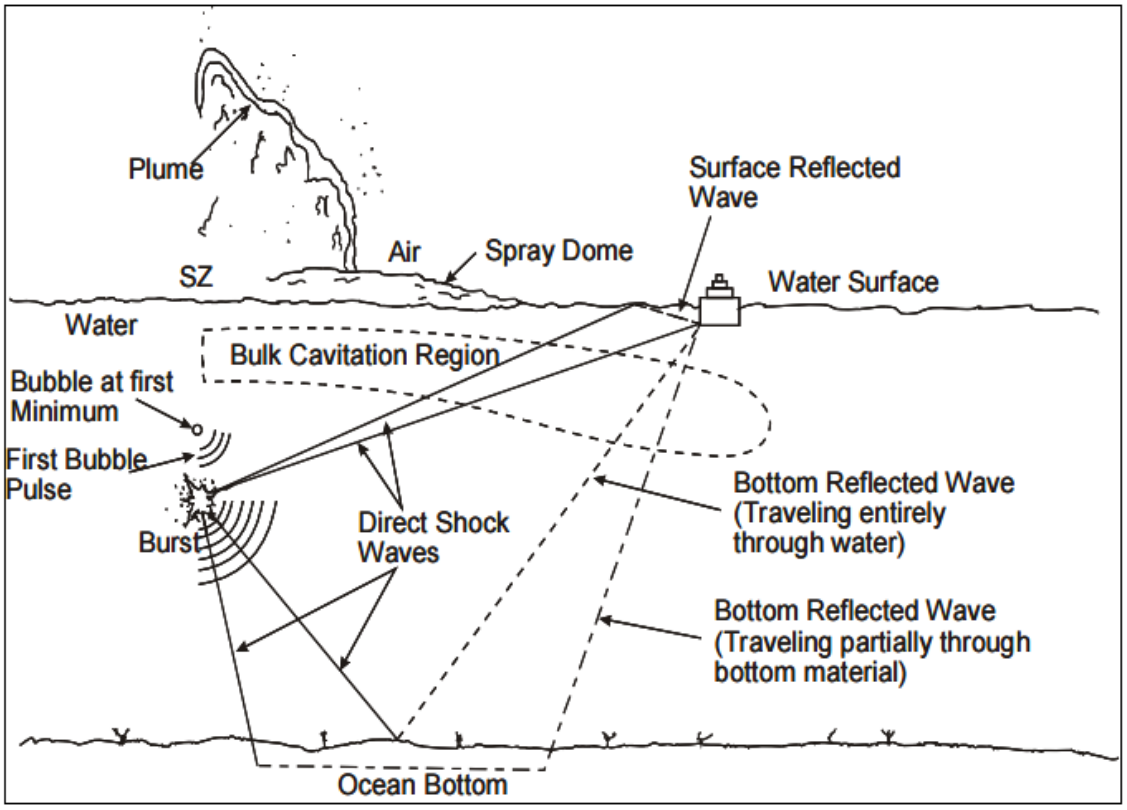

Figure 4. Complete summary of UNDEX. Source: [5].

III. BRIDGE STRUCTURE

A. TYPES OF BRIDGES

Bridges are critical to the physical and economic well-being of a community. They allow many different types of people to commute to and from work and also allow goods to move across waterways without the burden of hiring a ship. Because of the variety of location and available materials, there are a multitude of styles of bridge. That being said, there are four generally accepted categories of bridge: the beam bridge, the truss bridge, the arch bridge, and the suspension bridge. Examples of these types of bridges are shown in Figures 5 through 9.

1. Beam Bridge

Beam bridges, also known as girder bridges, are the simplest kind of bridge. In its most basic form, a log across a creek is a type of beam bridge [6]. When loaded, the top surface of the beam is compressed and the bottom is subjected to tension. As the bridge becomes longer and the supports spread apart, other supports are necessary to avoid bridge collapse. That being said, beam bridges are typically shorter than 76.2m (250 feet). When they do extend longer distances, a pier or other point connecting the bridge to the ground must be built to join multiple bridges together. This is termed a “continuous span” [7]. Beam and girder bridges are built using a series of beams or girders, typically and I-beam or a box girder.

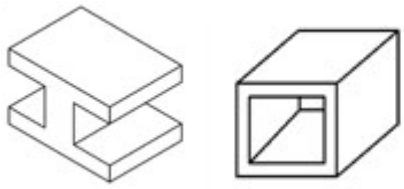

Figure 5. Diagram of I-Beam, left, and box girder, right. Source: [7].

A beam bridge is very stiff due to the increased moment of inertia from the I-beam and box girder and, as a result, can support the twisting and bending of a load.

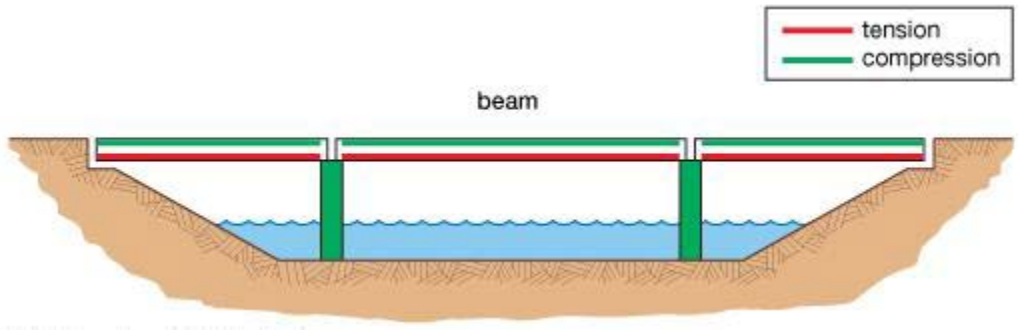

Figure 6. Diagram of beam bridge showing the locations of compression and tension. Source: [8].

2. Truss Bridge

A truss bridge leverages the strength of triangles to create a diagonal mesh above the roadway of the bridge. Because of the complexity of the structure, truss bridges are typically straight. They are fairly easy to construct because it is comprised of a series of small beams. Additionally, they can span long distances because of their incredible load bearing abilities. Different truss types will be used depending on the distance of the span. That being said, steel is almost always used to build a truss bridge.

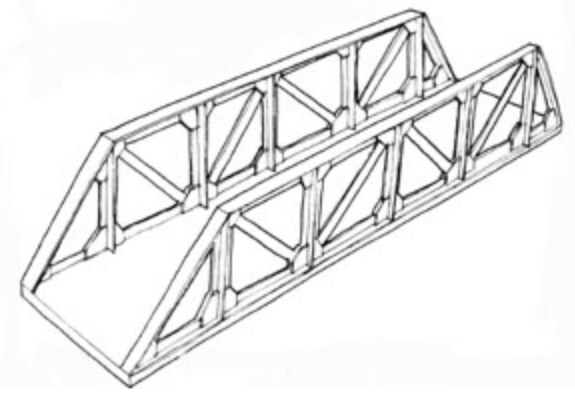

Figure 7. Representation of typical truss bridge. Source: [6].

3. Arch Brige

This type of bridge employs arches as the main structural component. Because of the curved structure, arch bridges have a high bending force resistance. When the bridge is loaded, a horizontal force translates to the ends of the arch. As a result, the ends of the arch have to be fixed in the horizontal direction, requiring a firm foundation on which the bridge is built. To mitigate any excessive force on the foundation, a system of hinges can be used. Two hinged arch types are the most common because they allow rotation, meaning that only horizontal and vertical forces are felt on the foundation. Arch bridges typically span less than 243.8 m (800 feet).

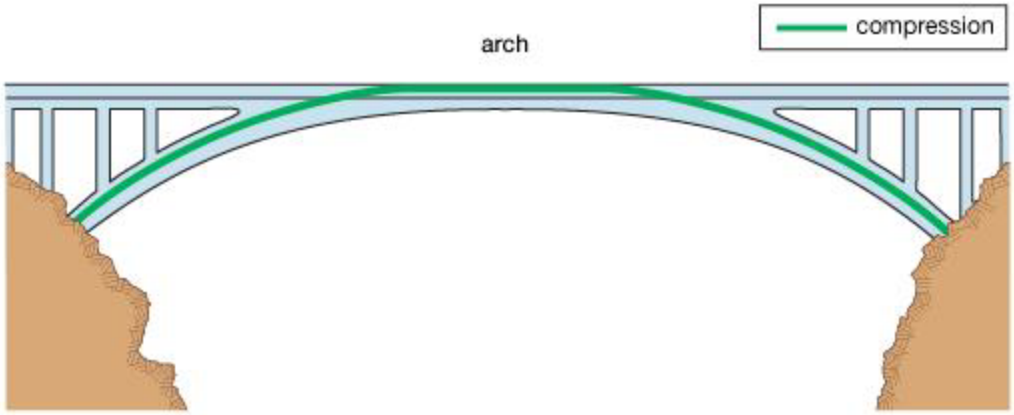

Figure 8. Arch bridge with lines showing compressive force. Source: [8].

4. Suspension Bridge

Suspension bridges have the potential to span the furthest out of any of the bridge types. Towers are built in the middle of the waterway and cables stretch down from the top of the tower to support roadway, known as the deck. Steel cables are almost always used and are very strong, but also flexible. As a result, a certain degree of motion can be expected in a suspension bridge. The cables will also extend onshore and be built into anchorages that help support the weight of the deck. Suspension bridges are typically the longest type of bridge because of their flexibility in construction. They could hypothetically extend forever so long as there are enough towers and the anchorages are massive enough to counter the load on the deck.

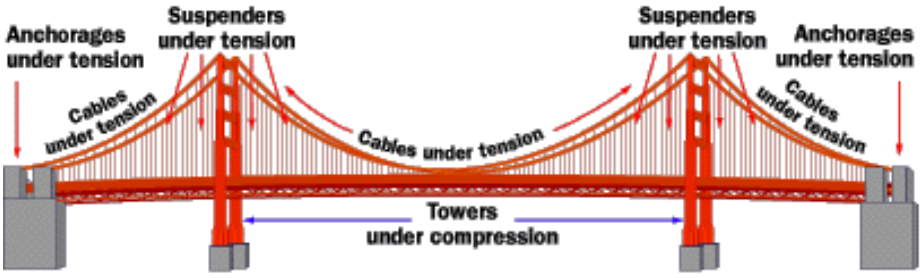

Figure 9. Diagram of typical suspension bridge. Source: [9].

B. FOUNDATION CONSTRUCTION

The foundation of a bridge presents some of the greatest challenges in bridge construction because of the innate degree of uncertainty. As a result, the foundation typically takes the longest time to build and also requires the greatest amount of research before construction [10]. The foundation refers to the element of the bridge that exists underground. Thorough studies on the soil must be completed to determine the soil hardness and if the soil is homogenous throughout the construction site. Depending on the soil and the nature of the body of water, five different methods can be used to build the deep foundation of the bridge: piles, cofferdams, open caissons, pneumatic caissons, and laid down caisson. This section will outline the basics of each of these methods and show key components in Figures 11 through 14 .

1. Piles

Piles are linear elements that transmit the load of the bridge into the deep soil. By driving the pile deep into the ground, the pile will become embedded in a hard surface, which will better bear the burden of the bridge. If the soil is not hard enough to bear the weight of the structure, the friction of the length of the element will distribute the load of the bridge to the ground soil. Piles may also be necessary if the waterway is subject to regular flooding, which will wash away significant portions of the ground soil.

Piles can be built in a factory and transported to the construction site or they can be built directly into the ground. If a pile is imported to the construction site, the pile is placed in the ground using a method called pile driving. Pile driving consists of forcing the pile into the ground either by hammer or by compressed air. In the latter case, a long

hole is made, then the reinforcement is placed in the hole, which is eventually filled with concrete [11]. Figure 10 shows the process in a land based construction situation.

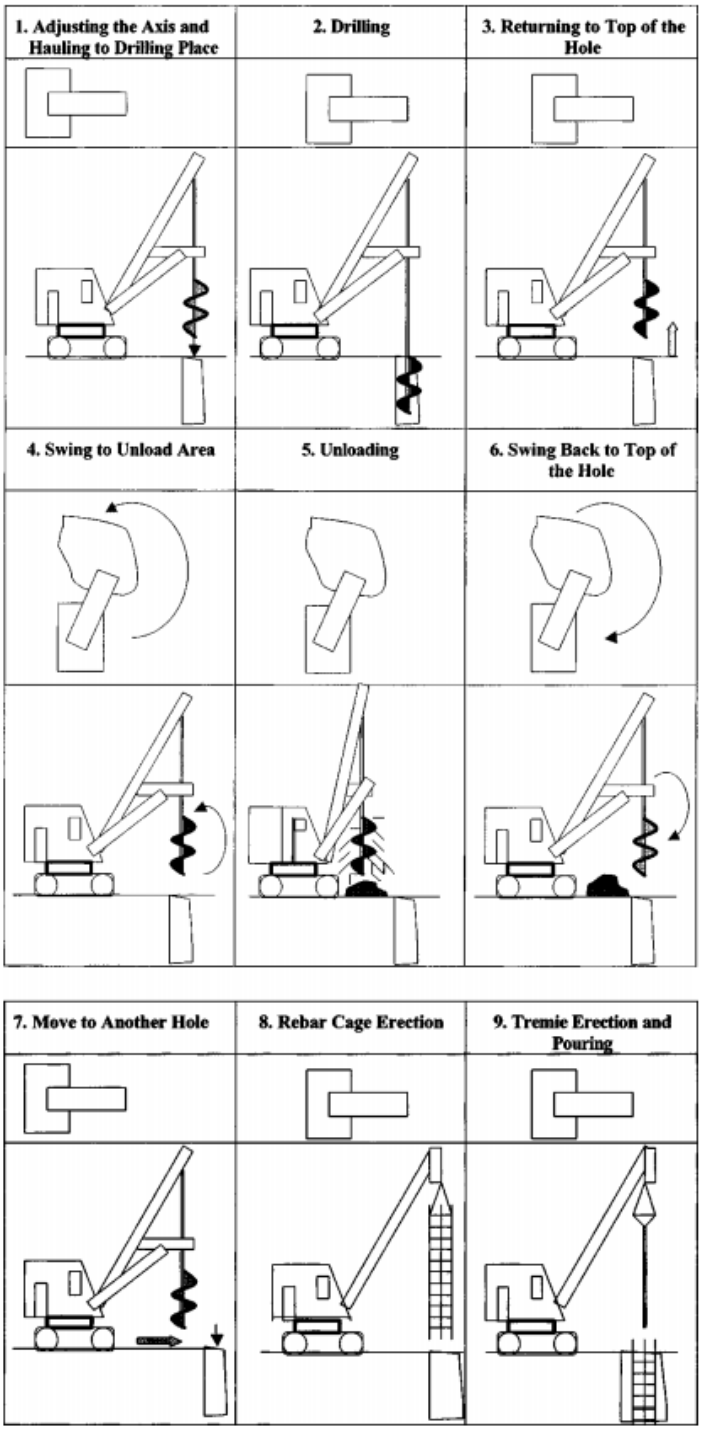

Figure 10. Process of constructing a pile on site. Source: [12].

2. Cofferdams

Cofferdams are enclosures used to keep water out of the construction area when the site is below the water line. There are multiple methods of constructing a cofferdam, but the essence remains the same: create a water tight space by driving walls into the ground then pumping the water out of the cordoned off area. Once the water is pumped out of the area, the foundation can be built in a dry environment. It is worth noting that the water will have to be continually pumped out of the interior because water will be drawn to the surface through the building of the foundation [13]. Once the foundation has been built, the cofferdam will be flooded and the enclosure removed. Figure 11 depicts a double walled steel cofferdam with gravel fill. Gravel is a popular fill material in cofferdam walls because it is economic and heavy enough to keep water from collapsing the structure.

Figure 11. Cofferdam with sheet metal walls and gravel filling between the walls. Source: [14].

3. Open Caissons

Similar to cofferdams, open caissons involve the clearing of an area inside of an enclosure, but with this method, the enclosure is part of the foundation. As the foundation is built inside the caisson, the caisson will slowly sink into the ground. In anticipation of this movement, caissons have a sharpened lower edge to speed the sinking. Once the caisson has reached the predetermined sunk level, the bottom will be sealed or the inside will be filled so that loads can be transmitted through the structure.

Open caisson is a very popular foundation method because it allows for creative foundation shapes. Typically, the enclosures are made of concrete cylinders to withstand ground thrusts. That being said, there is a great deal of flexibility in the enclosure construction, which is why this method is so popular.

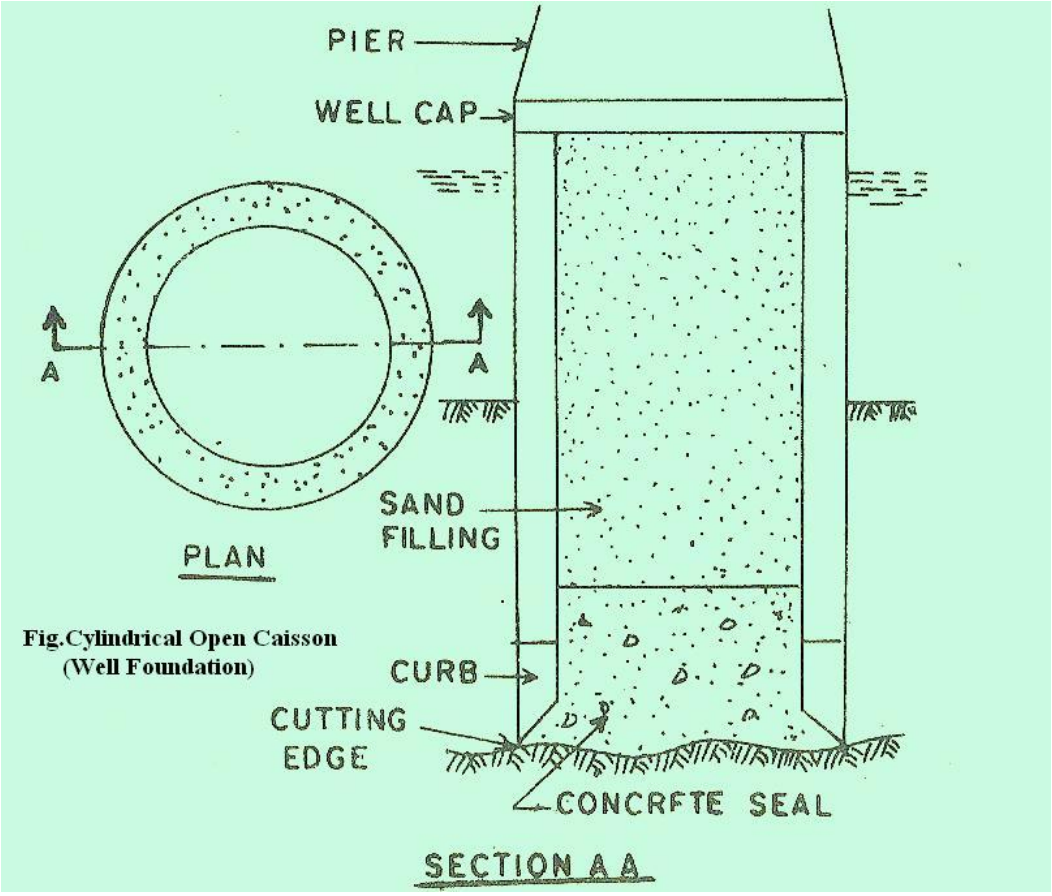

Figure 12. Diagram of an open caisson after it has been converted to a bridge foundation. Source: [15].

4. Pneumatic Caisson

Pneumatic caissons are closed at the top and open to the soil at the bottom. The caisson is sealed using compressed air to keep the water out and is accessible via two airlocks. One airlock takes workers down to the soil level while the other transports soil out of the excavation area. Similar to open caissons, the caisson is meant to sink into the soil and eventually act as a foundation for the structure. With a pneumatic caisson, the worker's removal of the muck means the caisson sinks faster into the soil.

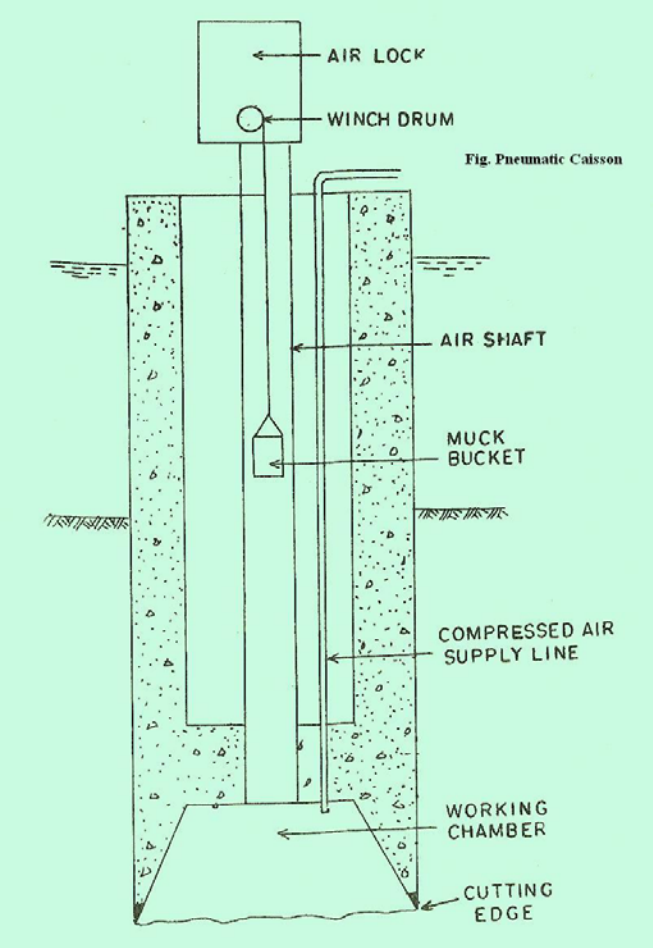

Figure 13. Diagram of pneumatic caisson that uses air lift to remove muck from the work site. Source: [15].

5. Laid Down Caissons

Laid down caissons can be used when the bottom soil is able to directly support the load of the bridge. An area at the bottom of the water way is prepared for the foundation and the caisson is pulled out to the site using tugboats. The floating caisson is then positioned directly over the cleared area and sunk to the bottom. The caisson can have either an open bottom or completed supports. This method is popular in offshore oil platforms.

There are also instances that a laid down caisson can be used when the soil is not capable of supporting the bridge load. When this is the case, the caisson will be lowered then piles driven from the water level. Eventually concrete is used as a bottom seal and pile cap allowing the water to be pumped out of the caisson interior.

C. PIERS AND ANCHORAGES

After the foundation has been laid, piers will be built that will eventually support the superstructure of the bridge. Previously, timber was the most common building material for piers; however, these piers rapidly deteriorated and in some cases became swollen with water [16]. As a result, modern piers are made of concrete to prevent corrosion in the harsh marine environment. In the case of suspension bridges, the piers will rise up and become the towers that will support the superstructure via cables. The cables will also be supported by anchorages on either side of the waterway. The anchorages act as their name suggests: large structures that counter the weight of the deck and hold the main cables in place. Anchorages are simply concrete blocks that house the ends of the cables and ensure that the weight of the bridge is evenly distributed across the ground. Figure 14 shows how all of the components relate to each other to form a complete suspension bridge.

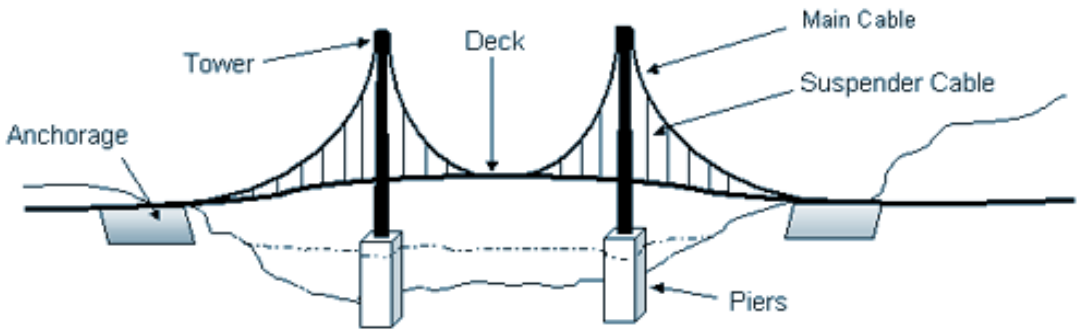

Figure 14. Diagram of elements of a suspension bridge. Source: [17].

D. FAILURE MITIGATION

Regardless of the myriad of good practices and preparation for construction, there will inevitably be flaws in the construction of bridge foundations. To mitigate these flaws, non-destructive integrity tests are performed to ensure the safety of the structure. The three traditional methods are low strain pile integrity tests, cross-hole sonic logging (CSL), and gamma-gamma logging (GGL). Low strain integrity tests consist of hammering the top of the foundation to generate a wave that will travel to the bottom of the foundation and reflect back to the top [18]. Any gross discrepancies in the cross sectional area of the foundation will cause a deflection in the wave and will show in the reflection readings. CSL requires two tubes be built into the foundation to allow an ultrasonic transmitter and receiver to be sent down the shaft. Based on the return, the receiver will be able to determine concrete quality throughout the foundation. GGL is very similar to CSL except radioactive material is sent down the tubes instead of an ultrasonic transmitter. A counter is used in place of a receiver and will be able to determine the density of the concrete based on the gamma rays received [18].

E. FAILURE OF CONCRETE BRIDGE PILINGS

Concrete presents unique challenges when developing failure models given its heterogeneous composition. Slight variations in the composition, curing temperature, and humidity can also have a massive impact on the material properties of a structure. These tenants make concrete particularly challenging because scaling is non-linear. As recently

as 2013, there have been calls to reevaluate the methods used in testing and quantifying the failure of concrete [19], [20].

There has been little effort to study concrete in uniaxial compression because that is when concrete is strongest. Tension and shear, on the other hand, are much more interesting because they almost always lead to the cracking that leads to the failure. Flaws in the form of cracks are innate to most concrete systems. In light loading cases, these cracks grow slowly and eventually stop propagating all together as the energy leaves the system [19]. When the load is heavy enough, the cracks grow rapidly and do not have a linear stress-strain response. Newman defines this load as the "discontinuity point" [22]. In 1963, Kaplan further characterized the crack propagation by showing that tensile strains served as a better predictor for the discontinuity point in flexure, splitting, and compression tests [21]. Since Kaplan's testing, his results were validated by Lowe in 1978 [22].

When modeling the failure of the bridge, critical assumptions are made about the failure criteria. The first assumption is that concrete will be linear to account for creep. The creep will be characterized by the elastic modulus from the load history. The second assumption is that the bridge will fail in tension as a result of tensile strain. Eyre and Nasreddin updated Newman's discontinuity point to be a strain limit because it represents a fracture caused by heavy enough loads such that the fracture propagates continuously [23]. Considering these assumptions, the relationship arises:

$$\varepsilon_2 = \frac{\sigma_2}{E} - \nu\frac{\sigma_1}{E} - \nu\frac{\sigma_3}{E} \tag{1}$$

where ε_2 is the principal stress direction and, at failure,

$$\varepsilon_2 = \varepsilon_t \tag{2}$$

The critical failure load, $\sigma_3 = f_c$ occurs when $\sigma_2 = \sigma_3 = 0$:

$$f_c = -\frac{E\varepsilon_t}{\nu} \tag{3}$$

DYSMAS takes this failure prediction method one step further by modeling the concrete as a matter of plastic flow. The implementation of this method is further described in Section B.2. The continual crack propagation of concrete is ultimately what

makes it so dangerous after any type of IED because of potential secondary failures that may occur after the initial detonation. As a result, any complete study of a concrete structure must include a post-detonation analysis.

IV. MODELING IN DYSMAS

The computer modeling system used to predict the effects of an underwater explosion is DYSMAS. DYSMAS is a fully coupled Eulerian-Lagrangian hydrocode that simulates an UNDEX in the three dimensional space. There are three components to the DYSMAS software shown in Figure 15: Gemini, the Eulerian component used to resolve the fluid; Dyna_N(3D), the Lagrangian component used to resolve the structure; and the Standard Coupler Interface (SCI), which synthesizes the results of both solvers at the end of each Eulerian time step to keep the continuity of the simulation [24]. It is worth noting that other Lagrangian solvers can be used in place of Dyna_N(3D), such as RigidBody; however, Dyna_N(3D) was the only solver employed for this study.

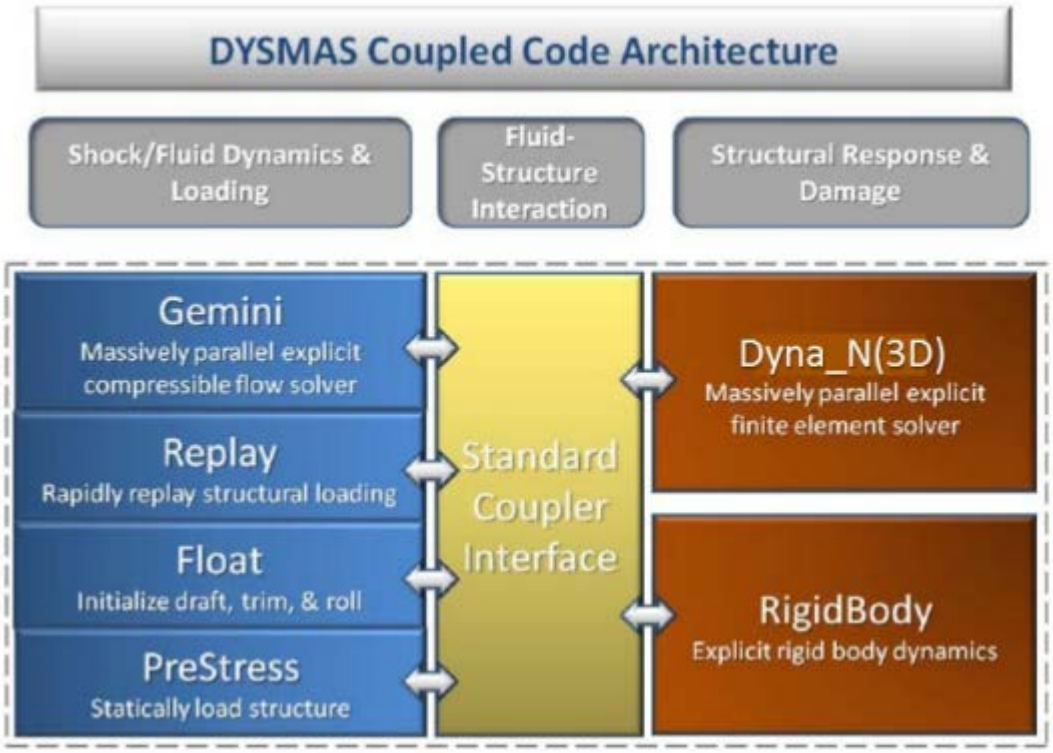

Figure 15. Diagram of DYSMAS architecture, which shows the relationship between GEMINI, Dyna_N(3D), and SCI. Source: [25].

A. GEMINI

Gemini employs the finite difference method to iteratively solve the Euler equations. Gemini is particularly powerful in the UNDEX environment because it is specifically designed to capture aspects of shockwaves and bubble jetting. It can solve flow fields with a variety of fluids. The Float and PreStress options of the Gemini program have the capability of positioning and pre-stressing a model before the start of the simulation.

1. Theory

Gemini solves the fluid mesh to first order accuracy by applying the Godunov method algorithm at each time step. Subsequently, the algorithm is applied to the individual Euler cells in each principal direction through a one dimensional approach. By breaking down the different directions to unit vectors, the Euler equations can be solved by conservation of mass, momentum, and energy. That being said, one of the downfalls of applying the Euler equations is the assumption of inviscid flow. Most solids can support shear loading, however, the frictionless flow assumption inhibits Gemini's ability to accurately model a Lagrangian solid bottom [26].

2. Components

There are three components to the Gemini program: Pre-processing, the Main Program, and Post-Processing. The relationship between the three elements is shown in Figure 16. The light blue boxes are user-defined input files required to implement the program.

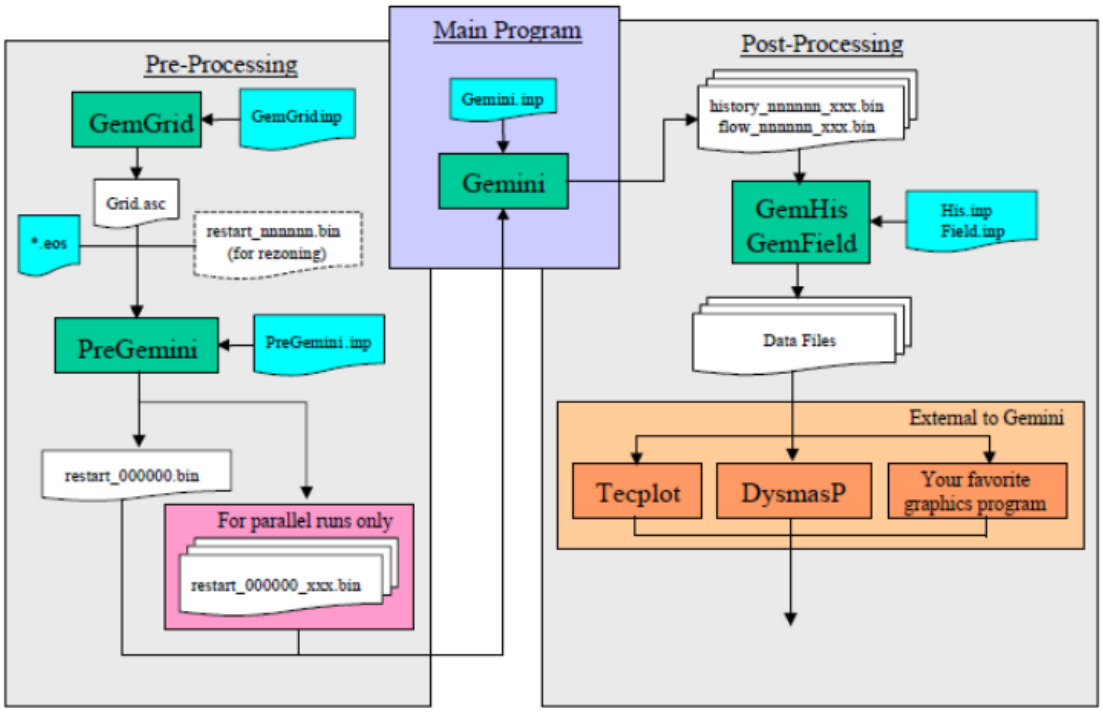

Figure 16. Diagram of relationship between GEMINI components
Source: [25].

3. Pre-Processing

The primary function of the pre-processing stage of Gemini is to fully characterize the environment in which an UNDEX occurs. This requires the user to establish a coordinate grid, the environment (explosive, air, water, soil, etc.), and any parallel processing that will occur. In regard to the coordinate system, Gemini can set up a one, two, or three-dimensional system with spherical, cylindrical, or Cartesian coordinates. After deciding on a coordinate system, the flow field is generated using GEMGRID. GEMGRID can have either user defined cell sizes or uniform cell sizes, which is the default setting. The generation of the grid is independent in every direction. Additionally, GEMGRID has the ability to quicken computational time by allowing cells away from the structure to be larger because they are less critical to the results.

After the completion of GEMGRID, PREGEMINI models the physical environment. The user will define critical features such as the depth of water and the charge type, weight, and location. PREGEMINI can also ‘rezone’ flow fields to things

like modeling a cylindrical 2-D calculation into a 3-D Cartesian system or break down the domain into subgrids that can be used for multiple processing.

4. Main Program

The main processing of Gemini uses the outputs of PREGEMINI and user specified inputs to generate GEMHIS and GEMFIELD. The user defined inputs indicate things like whether the simulation includes a solid in addition to the fluid, element histories, termination parameters, and other critical factors. If there is a solid involved in the simulation, then it is a coupled calculation and the Dyna deck is initialized in tandem with Gemini. The output data from Gemini will create GEMHIS and GEMFIELD, which will be further discussed in Post-Processing.

5. Post-Processing

Post-processing leverages the data outputs of Gemini to generate plot files from a number of visualization programs. GEMHIS is a time history of points that were identified in the Gemini input deck. These points can be anything ranging from structural nodes, to whole elements, to points in the flow field. Further, various types of histories can be extracted from these points including pressure, velocity, and a number of other critical aspects. GEMFIELD creates data records over a user defined period of time for a specific variable, which can be used to create a series of plots that are strung together into animations of the subdomain.

B. DYNA_N(3D)

Dyna_N(3D) evaluates the structural response to the UNDEX using a Lagrangian solver. Like Gemini, Dyna_N(3D) employs three-dimensional finite elements in its analysis.

1. Theory

The software can solve both linear and non-linear systems using the second order differential equation of motion. Equation 6 is the linear formulation and Equation 7 is the non-linear.

$$m\ddot{x} + c\dot{x} + kx = p(t) \tag{4}$$

$$m\ddot{x} + c\dot{x} + f_{int} = p(t) \tag{5}$$

The combination of these two equations is as follows:

$$[M]\{\ddot{x}\} + \{F\} - \{P\} = 0 \tag{6}$$

where [M] is the mass matrix of the structure, $\{\ddot{x}\}$ is the acceleration, {F} represents the internal non-linearity and {P} is the body forces and external loads [27].

Employing these equations, a central differencing scheme is used to step through time. It is vital that the time step remains below the Courant number so the solution can be stable. In other words, the user must ensure that the time step is small enough to allow the program to analyze the wave as it propagates through each element. Given how fast the shock waves will move and how detailed the analysis must be, the maximum time step will be dictated by the smallest element in the structure. The Standard Coupler Interface will help in deciding the time step by choosing the smaller between Gemini and Dyna_N(3D) [28].

2. Pre-Processing and Post-Processing

DYSMAS Pre-Processor 2010 allows the user to build the structure for analysis. The Pre-Processor also has the ability to assign material properties to the structure, define boundary conditions, apply body forces and determine the fluid-structure interface. Once the model is built in the Pre-Processor, it will be written into the appropriate input cards for Dyna_N(3D) [1].

The post-processor is a tool to visualize the fluid-structure response to the UNDEX. Similar to Gemini, aspects of the structures response can be extracted and replayed for analysis.

C. STANDARD COUPLER INTERFACE (SCI)

The SCI is the key component to DYSMAS because it fully couples the Eulerian and Lagrangian simulations. By passing information between the fixed Eulerian grid and

the finite element model whose components move, the simulation can capture the nuances of an UNDEX. The primary functions of the SCI are [26]:

- Instill the structural interface in grid form on the Euler mesh
- Maintain boundary conditions and the fluid-structure interface
- Activate or de-activate elements as the fluid-structure interface moves through the Euler mesh
- Determine loads at the nodes.

V. DEVELOPMENT OF PARAMETRIC MODEL

The initial stage of testing consisted of three parametric studies to determine (1) the most critical water level for a waterborne IED and (2) bearing load sensitivity and (3) reinforcement volume fraction sensitivity of the foundation. For the first study, the water height will be varied along with the horizontal standoff distance to determine which situation will cause the most damage to a generic foundation. The second study will vary the load on the same foundation to determine how sensitive the foundation is to changes in the load. The final study will vary volume fraction and orientation of the reinforcement in the structure, again to determine how sensitive the foundation is these changes.

A. ENVIRONMENT

When building the testing environment in DYSMAS, the user should build as small an environment as possible that allows them to accurately capture the impact of the explosion on the foundation. As such, the surrounding sand, water, and air is only deep enough to study the foundation through the sand and only tall enough to examine any refraction from the air back into the water. Making the simulation runs computationally inexpensive is the driving factor behind the dimension of the environment, two of which are shown in Figure 17. The depth of the sand and water are based off of preliminary information gathered about a known bridge. The material properties of the air, water, and sand have been tested for their accuracy. Figure 17 shows the sand in blue, the water in yellow, and the air in pink. All of the material inputs can be found in Appendix A.

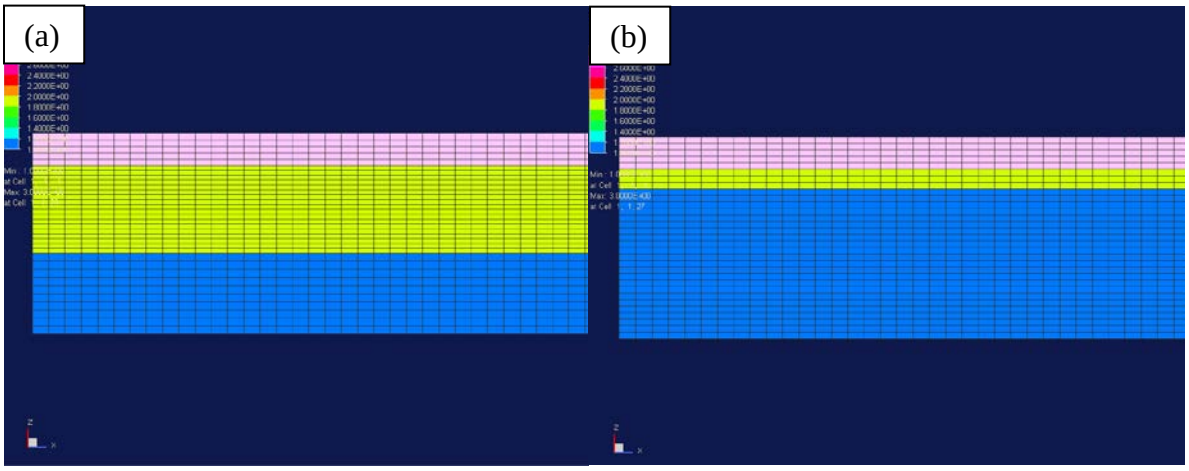

Figure 17. In the image, (a) shows the deep-water boundary condition while (b) shows the shallow water condition.

1. Sand

The sand is modeled with the P-α equation of state, which is an equation used for porous materials, and the Mie-Grüneisen equation of state, which eliminates air-filled voids in the sand. This is a first order theory in which irreversible compression of the material takes priority over the shear effects [29]. The parameters of this material are shown in Table 1. The first portion of Table 1 are solid material properties, while the latter (P_s, P_e, α_0, C_e^2) are porous material properties.

Table 1. Properties of sand for P- α equation of state. Source: [29].

DYSMAS P-α Parameters	
Γ_0	Grüneisen gamma
S	Shock speed of the solid material
ρ_0	Datum density of the solid
e_0	Datum energy of the solid
p_0	Datum pressure of the solid
C_s^2	Reference sound speed of the solid squared
P_s	Pressure for all void elimination
P_e	Initial elastic pressure threshold
α_0	Initial solid density/ initial porous density
C_e^2	Virgin porous material sounds speed

Figure 18 shows the values assigned to the variables in Table 1. Please note that all of the simulations were run in English Engineering units (lb., ft., s).

```
<EOS VARS>
  gamma0=.96299999952
  S=1.8600000143
  rho0=0.13014274e+00
  ei0=0.0
  p0=4.036e+00
  c02=2.5197e+05
  ps=1.81297e+03
  pe=0.0
  alpha0=1.05195669
  ce2=4.31e+5
<END EOS VARS>
```

Figure 18. Values used for sand properties. Source: [30].

As stated earlier, the sand was only large enough to capture the scope of the UNDEX's impact on the foundation. As such, the sand extended to the bottom of the foundation and no further. In the deep water condition, the sand consists of 8750 elements that are 1.52 m x 3.05 m x 3.05 m (5' x 10' x 10'). The intermediate water has 14438 elements that are 1.37 m x 3.05 m x 3.05 m (4.5' x 10' x 10'). The shallow water condition has 20125 elements that are 1.22 m x 3.05 m x 3.05 m (4' x 10' x 10'). These dimensions were chosen to be similar to the dimensions of the foundation. Similar dimensions will ensure that the Eulerian and Lagrangian simulations can properly couple.

2. Water

The water is modeled using the Tillotson equation of state. This equation allows for adjustment in the speed of sound via the constant *A*. The equation of state is:

$$p = p_0 + \omega p\left(e - e_0\right) + A\mu + B\mu^2 + C\mu^3 \tag{7}$$

$$\mu = \frac{\rho}{\rho_0} - 1 \tag{8}$$

$$\omega = \gamma - 1 \tag{9}$$

where γ is the ratio of specific heats, ρ_0 is the reference density, e_0 is the reference energy, p_0 is the reference pressure, and *A*, *B*, and *C* are constants. Three different water depths were used; 3.66 m(12 ft.), 10.36 m (34 ft.), and 16.46 m (54 ft.). For the deep water, there are 15750 elements that are 1.83 m x 3.05 m x 3.05 m (6' x 10' x 10'). The

intermediate depth water has 9188 elements that are 1.52 m x 3.05 m x 3.05 m (5’ x 10’ x 10’). The shallow water has 2625 elements that are 1.22 m x 3.05 m x 3.05 m (4’ x 10’ x 10’). The element size is based off the structure and was developed to make the interface of Eulerian and Lagrangian as smooth as possible [31].

3. Air

Gamma law is the equation of state used to model air. This equation takes the following form:

$$p = (\gamma - 1)\rho e \tag{10}$$

where γ is a user specified constant. For these tests γ is 1.4 to match the value used in previous simulations. For both deep and shallow water conditions the air is made of 4375 elements that are 1.22 m x 3.05 m x 3.05 m (4’ x 10’ x 10’). Again, these element sizes were selected to approximately match the size of the water elements [32].

4. Explosive Material

All of the simulations used TNT as the explosive material. TNT’s primary ingredient is toluene and is an inherently stable material. Its stability causes it to be prevalently used in military and mining applications, but also in IEDs. Additionally, this material is used to measure energy release, called TNT equivalent. As a result, the conclusions of these tests can easily be translated to other explosive materials [33].

DYSMAS models both the unburned and burned TNT material to accurately capture the environment during detonation. By leveraging the constant detonation velocity of the explosive and the size of each Euler cell, the simulation smoothly transitions the unburned material to the detonated state. The “Tait for Unburned Explosive” equation of state determines the behavior of the solid material. This equation has the form of the Tait equation of state, pressure is a sole function of density, shown in Equation 11.

$$p = p_0 + B\left(\left(\frac{\rho}{\rho_0}\right)^{\gamma} - 1\right) \tag{11}$$

where γ and B are constant Tait parameters, p_0 is the datum pressure, and ρ_0 is the datum density [34].

The burned material is described as a gaseous product. The simulation uses the JWL equation of state, shown in Equation 12. Note that the constants, A, B, R_1, R_2, ω, and ρ_0 can be found in in standard explosive reference guides [35].

$$p = A\left(1 - \frac{\omega\rho}{R_1\rho_0}\right)e^{-R_1\frac{\rho_0}{\rho}} + B\left(1 - \frac{\omega\rho}{R_2\rho_0}\right)e^{-R_2\frac{\rho_e}{\rho}} + \omega\rho e \tag{12}$$

For the depth study, the TNT has a radius of 0.305 m (1 ft.). The sensitivity studies have IED's of 0.0762 m (0.25 ft.) radius. Upon detonation, the difference in pressure between the explosive and the water is in the order of 1499 GPa (31.3 x10^6 psf), causing the wave shock wave to initially move approximately 1524 m/s (5000 ft./s).

B. FOUNDATION

The foundation will be 69.80 m x 39.32 m x 30.48 m (229' x 129' x 100') as seen in Figure 19. The foundation has 6171 nodes and 5120 elements. Each element is 4.36 m x 1.22 m x 3.048 m (14.3' x 4' x 10'). The elements are much finer in the y direction because the y-z face will have first contact with the shockwave, therefore the effects of the detonation will be accurately observed. Initial simulations have also shown that this is where the location of greatest deformation will be. The size of the elements in the x and z direction was driven by the need to have a mesh that will be accurate but not computationally expensive. There were some concerns that the rectangular shape of the element would cause elemental torsion; however, these concerns were dismissed after the foundation behaved as expected in preliminary simulations.

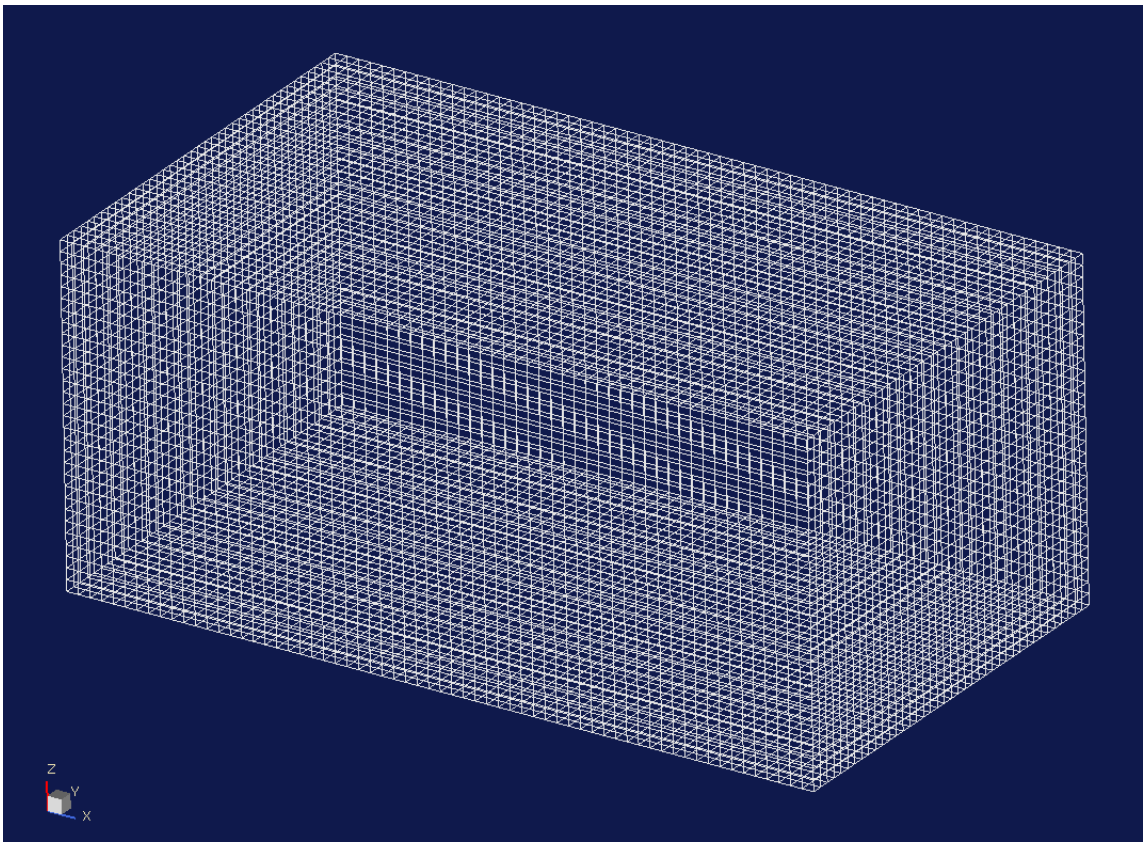

Figure 19. Bridge foundation and finite element mesh.

1. Coupling

In DYSMAS Pre-processor, the user must define the coupling interface between the fluid and structural elements. The program uses the standard coupler interface to track the coupled elements' interaction to the fluid in addition to their interaction with the rest of the structure. Figure 20 shows the coupled interface as purple boxes. Note that all of the arrows point out of the structure indicating that the fluid will be on the outside of the structure as opposed to contained within.

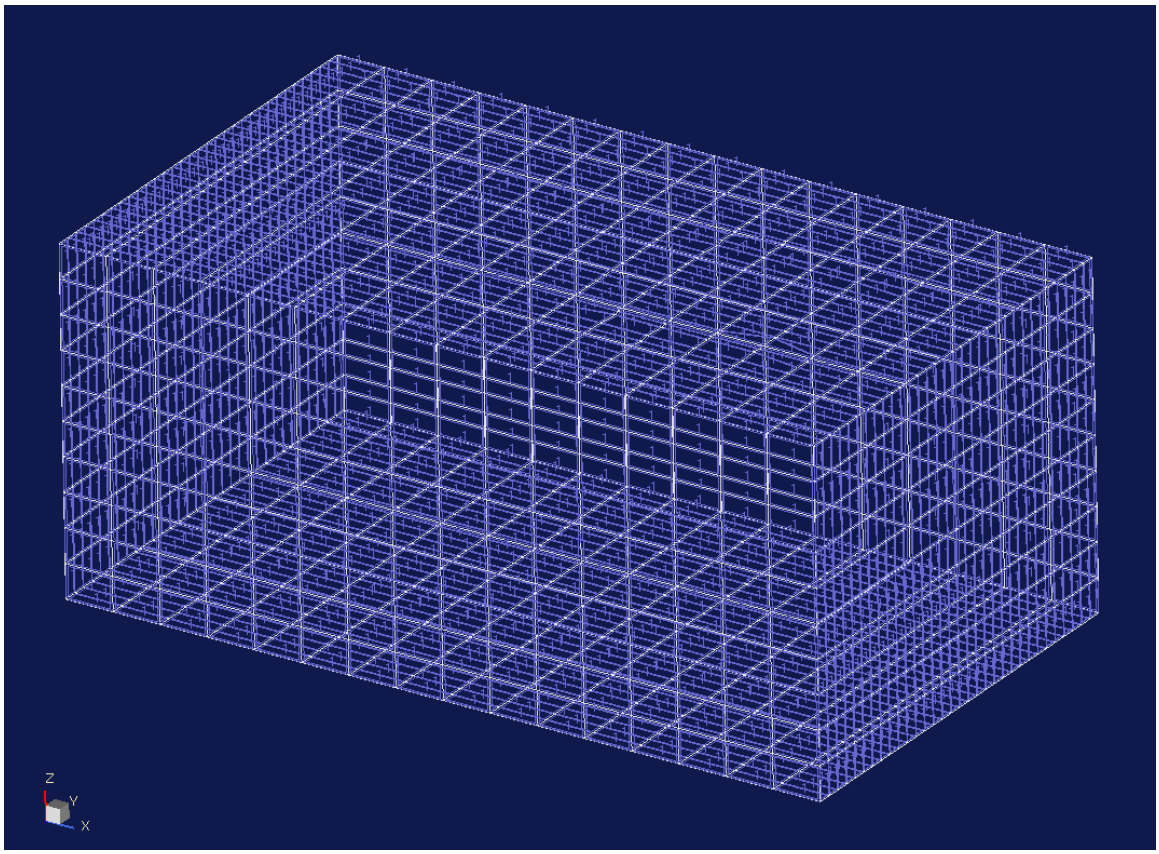

Figure 20. Coupled interfaces of foundation model

2. Concrete Modeling

To model unreinforced concrete, the initial stage of the parametric study used Material 45 ([36]). This material model was developed in 1996 to support the Defense Threat Reduction Agency's research programs. The failure of this model is a plastic flow controlled by a failure surface whose midpoint is determined by two of the three functions.

$$\Delta\sigma_y = a_{0_y} + \frac{p}{a_{1_y} + a_{2_y} p}\left(\textit{initial yield surface}\right) \tag{13}$$

$$\Delta\sigma_m = a_0 + \frac{p}{a_1 + a_2 p}\left(\textit{maximum failure surface}\right) \tag{14}$$

$$\Delta\sigma_m = \frac{p}{a_{1_f} + a_{2_f} p}\left(\textit{residual failure surface}\right) \tag{15}$$

When the stress point is between the initial yield surface and the maximum failure surface, the current failure surface is obtained via the following equation:

$$\Delta\sigma = \eta\left(\Delta\sigma_m - \Delta\sigma_y\right) + \Delta\sigma_y \tag{16}$$

where η is between 0 and 1 depending on the damage parameter, λ. When the stress point is between the maximum failure surface and the residual, the current surface is interpolated via

$$\Delta\sigma = \eta\left(\Delta\sigma_m - \Delta\sigma_r\right) + \Delta\sigma_r \tag{17}$$

The function $\eta(\lambda)$ is a series of 13 $(\eta\lambda)$ pairs. The damage parameter must start at 0 and increase over the course of the simulation. The variable η, which is a dummy integer used in the function, will also start at 0 and increase to 1 when λ is at its median value after which it will decrease to 0 at λ continues to grow. This parabolic relationship allows $\Delta\sigma$ to equal $\Delta\sigma_y$, $\Delta\sigma_m$, and $\Delta\sigma_r$. The damage scaling exponents, b_1, b_2 and the lambda-stretch factor, s, adjust the impact between the increments of the effective plastic strain and the damage parameter based on the following two equations:

$$d\overline{\varepsilon^p} = \sqrt{(2/3)\varepsilon_{ij}^{'p}\varepsilon_{ij}^{'p}} \tag{18}$$

$$d\lambda = \begin{cases} \dfrac{\overline{d\varepsilon^p}}{\left[1+\left(\dfrac{s}{100}\right)\left(r_f - 1\right)\right]\left(1 + p/r_f f_t\right)^{b_1}}, p > 0 \\ \dfrac{\overline{d\varepsilon^p}}{\left[1+\left(\dfrac{s}{100}\right)\left(r_f - 1\right)\right]\left(1 + p/r_f f_t\right)^{b_2}}, p < 0 \end{cases} \tag{19}$$

where r_f is the rate-enhancement factor and $f_{t.}$ is the static unconfined tensile strength. It is interesting to note that when the pressure is 0, the denominator is a continuous function, which allows the damage evolution to behave differently in tension and

compression. Also, the bracket term becomes 1 if s=0 and r_f if s=100. As such, if s=100, there is no lambda-stretch factor.

To model the failure of concrete more realistically, pressure decay is built in after isotropic tensile failure. Further, a damage increment impacts the volume when the path of the stress failure is close to the triaxial tensile test path. The ratio $(3J_2)^{\frac{1}{2}}/p$ defines the closeness to the triaxial tensile path and will ultimately determine the incremental damage to the structure as given by the multiplication factor f_d:

$$f_d = \begin{cases} 1 - \dfrac{\left|\dfrac{\sqrt{3J_2}}{p}\right|}{0.1}, \left|\dfrac{\sqrt{3J_2}}{p}\right| < 0.1 \\ 0, \left|\dfrac{\sqrt{3J_2}}{p}\right| \geq 0.1 \end{cases} \tag{20}$$

These various components combine in the following way to modify the effective plastic strain:

$$\Delta\lambda = b_3 f_d k_d \left(\varepsilon_v - \varepsilon_{v,yield}\right) \tag{21}$$

where b_3 is the input scalar multiplier, k_d is the internal scalar multiplier, ε_v is the volumetric strain, and $\varepsilon_{v,\,yield}$ is the volumetric strain at yield.

Another critical parameter is the fractional dilatancy parameter, ω, which is the initial ratio of the plastic volume strain increment to the volume strain increment if the plastic flow existed in a hydrostatic plane. The fractional dilatancy will not change until the stress point reaches the maximum failure surface, at which point ω will become 0. As the fractional dilatancy approaches 0, the effective fractional dilatancy is the initial value multiplied by η and edrop. Edrop is a user defined parameter that is used exclusively to govern the decay of the fractional dilatancy. If edrop=1, the post-peak dilatancy decreases linearly in relation to η and if edrop is 0, there is no decay until the stress point reaches the residual failure surface.

DYNA3D will also output a scaled damage parameter, δ, given by

$$\delta = \frac{2\lambda}{\lambda + \lambda_m} \tag{22}$$

which will be given as the effective plastic strain in the post-processor of DYSMAS [37].

The values input into Material 45 were based off of extensive testing conducted by Noble and Kokko. They used Material 45 to model the WSMR-5 ¾ concrete used in the Morrow Point Dam. Appendix B shows the required input values for the concrete modeled and Table 2 the numerical inputs. Figure 21 also shows a plot of the compressive meridians, a single element test, and a uniaxial unconfined compressive test.

Table 2. DNYA3D input for WSMR- 5 3/4 concrete. Source: [38].

CARDS	COLUMN 1	COLUMN 2	COLUMN 3	COLUMN 4	COLUMN 5	COLUMN 6	COLUMN 7	COLUMN 8
3	1.900E-01	4.640E+02	1.946E+03	4.463E-01	1.228E-05	1.500E+00	5.000E-01	4.417E-01
4	s=0 or 100	2.000E+00	0.000E+00	volumetric strain at failure	0.000E+00	load curve giving rate sensitivity	0.000E+00	0.000E+00
5	0.000E+00	1.000E-05	3.000E-05	5.000E-05	7.000E-05	9.000E-05	1.100E-04	2.700E-04
6	5.800E-04	7.800E-04	1.331E-02	5.000E-01	6.000E-01	1.150E+00	1.469E+03	6.250E-01
7	0.000E+00	8.500E-01	9.600E-01	9.900E-01	1.000E+00	9.900E-01	9.600E-01	5.000E-01
8	5.000E-02	1.000E-02	0.000E+00	0.000E+00	0.000E+00	1.600E-01	1.797E-05	3.981E-05

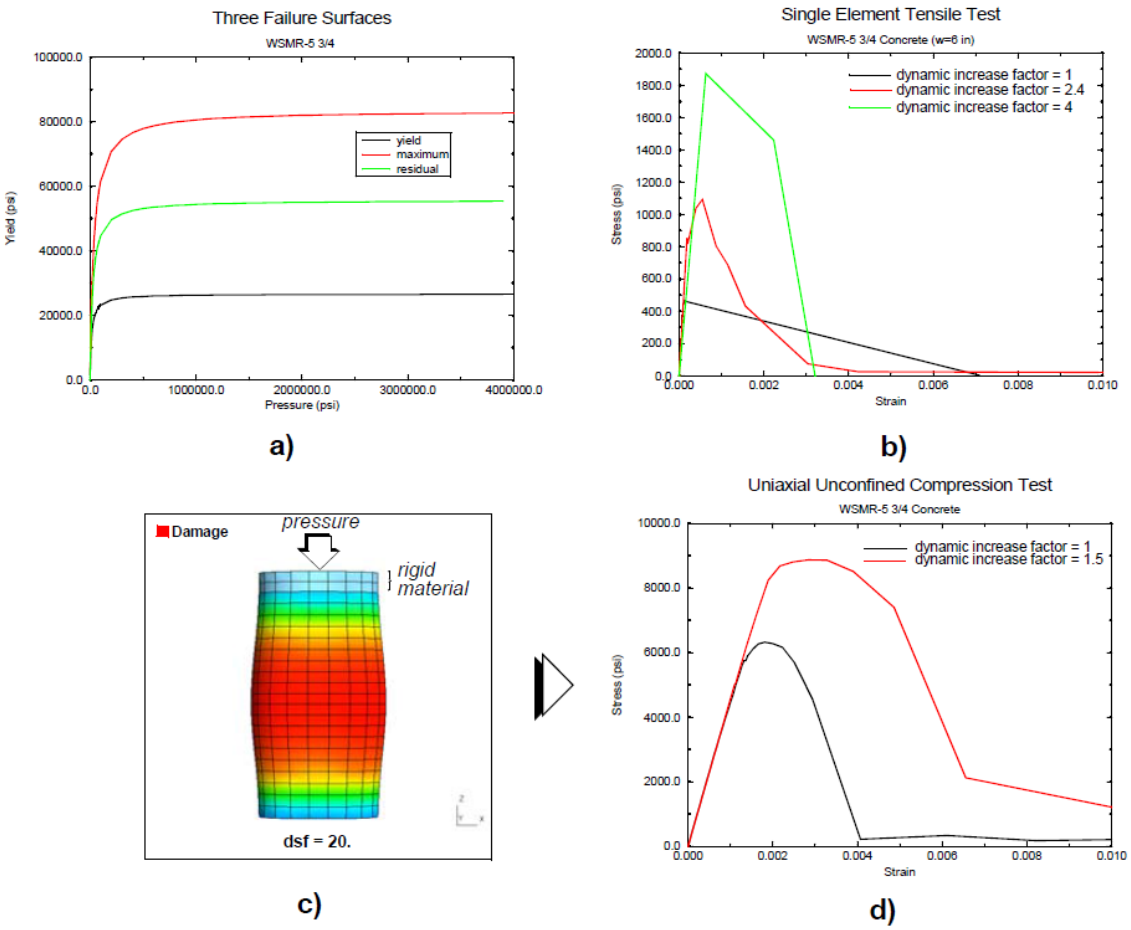

Figure 21. Plots of (a) the compressive meridians, (b) single element uniaxial test with and without rate dependence; (c) depiction of uniaxial compressive test; (d) stress-strain plot. Source: [38].

3. Reinforced Concrete Modeling

Material 66 is a modification of Material 45 to allow for the modeling of reinforcement in the concrete structure. This model has the same input setup of Material 45 and simply adds a few more parameters to accurately capture the behavior of reinforcement. The hardening of the rebar abides by the following power law:

$$\sigma_y = \sigma_0 \bullet \left[1 + \beta\left(\overline{\varepsilon}_p + \varepsilon_0 0\right)\right]^n \tag{23}$$

The strain on the rebar is determined by the following:

$$\sigma_y = \sigma_y \bullet \left[1 + \frac{\bar{\varepsilon}_p}{\varepsilon_{ref}}\right]^m \tag{24}$$

4. Equation of State

Equation of state 8 dictates the relationship between pressure and volumetric strain while also tracking the unloading bulk modulus, *K*, at peak volumetric strains. Interestingly, DYSMAS describes pressure as positive in compression and volumetric strain as positive in tension. The relationship between pressure and volumetric strain will have a cubic spline representation as shown in Figure 22.

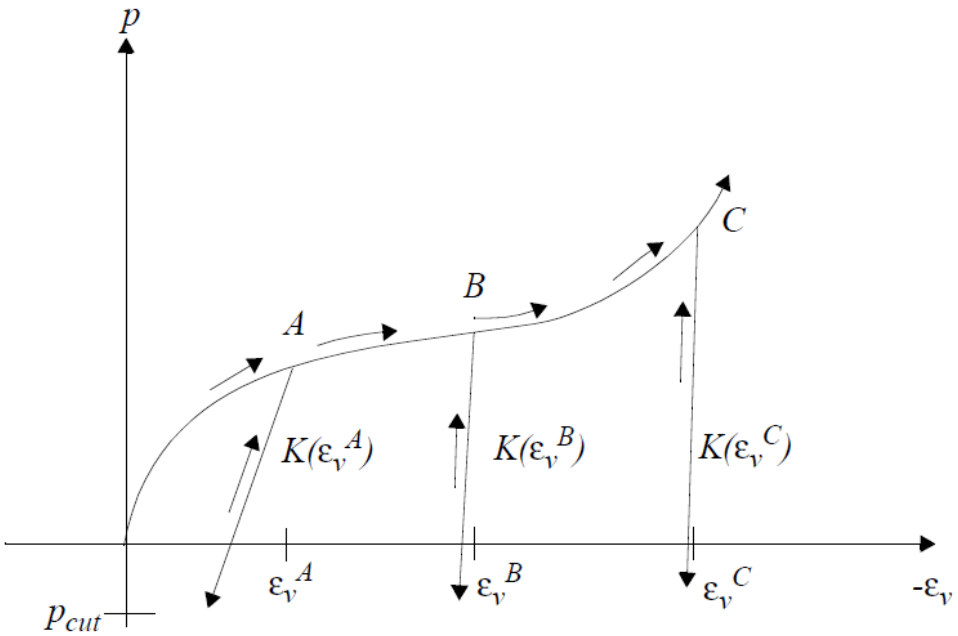

Figure 22. Pressure versus volumetric strain. Source: [38].

The input values for the equation of state are shown in Appendix B.

VI. DEPTH STUDY RESULTS

To determine the most critical depth of detonation, the damage parameters at a single time step were compared. To ensure the detonation fully impacted the foundation, the effective stress of each run was examined. The effective stress is the intergranular pressure of the foundation; therefore, as the foundation experiences the pressure from the bomb, the stress will increase to keep the grains from collapsing onto each other. Because the foundation has the same dimensions and material properties, the force of the material acting on itself should be the same for all. Figure 23 shows a typical graph of the effective stress. The stress increases rapidly as the pressure from the detonation moves over the foundation and then asymptotes.

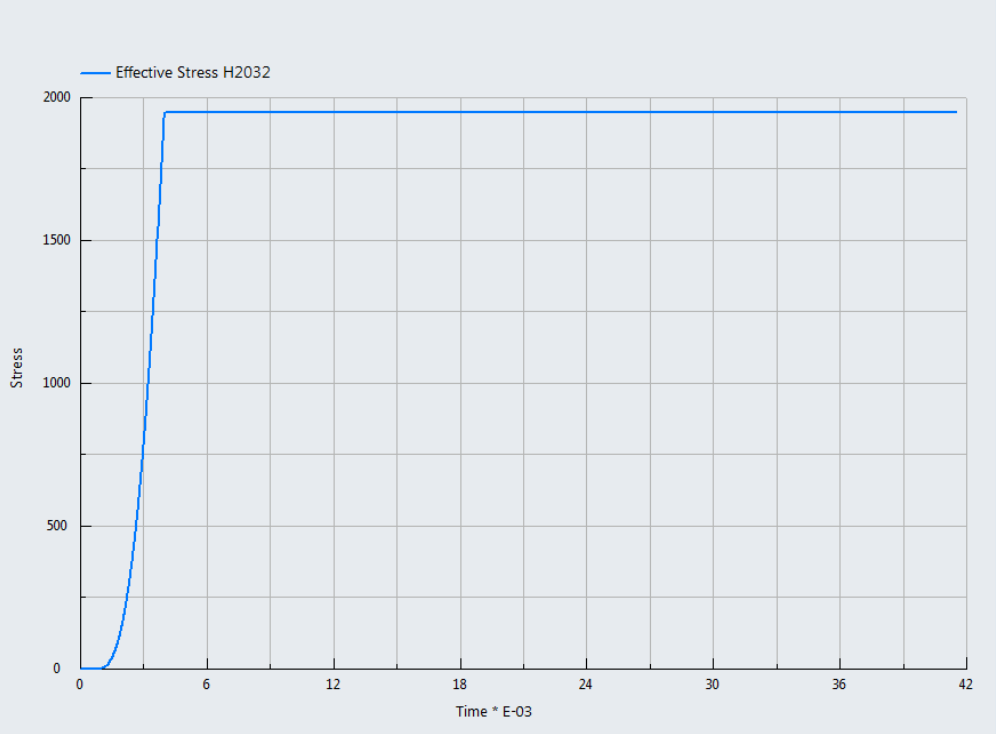

Figure 23. Effective stress on element 2032 when the bomb is detonated at 6.096 m (20’) from the foundation in 3.66 m (12’) of water.

The effective plastic strain was also examined to ensure that it reaches an asymptote, signaling the bombs impact on the foundation. Figure 24 shows a typical graph of the effective plastic strain. The effective plastic strain increased rapidly, though not as rapidly as the effective stress, and converged after the detonation. The effective plastic strain will be normalized using Equation 22 to derive the damage parameter.

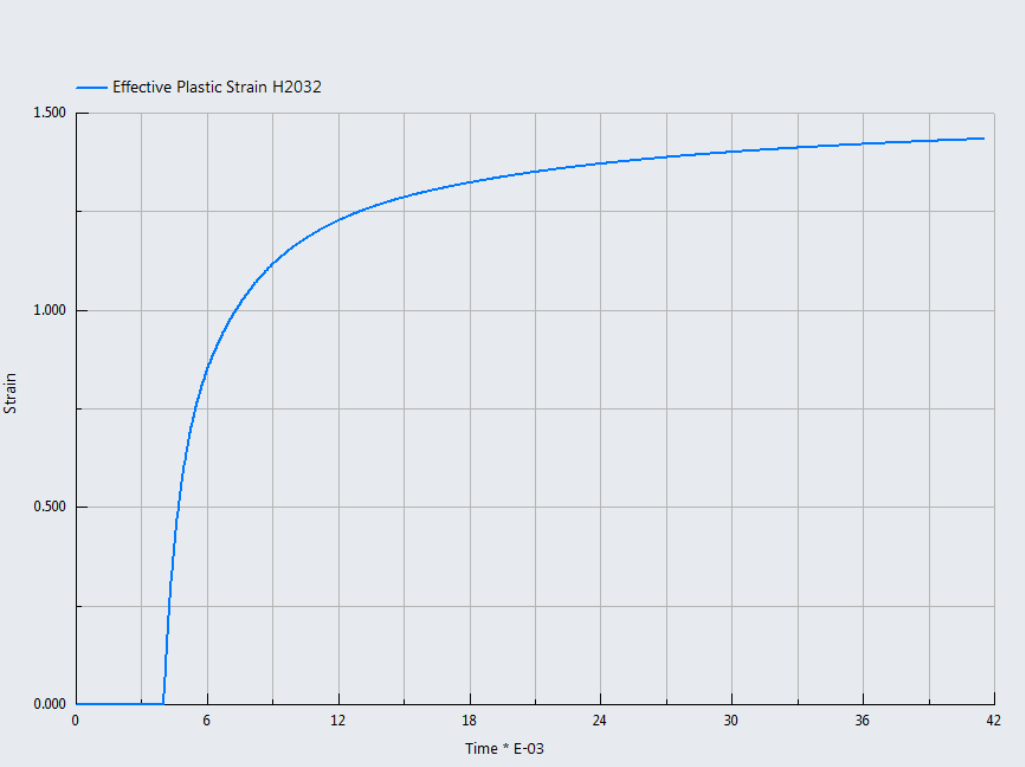

Figure 24. Effective plastic strain on element 2032 when the bomb is detonated 6.096 m (20') from the foundation in 3.66 m (12') of water

A. DAMAGE PARAMETER

Concrete will continue to degrade long after the detonation because of its ability to crumble. As such, the damage parameter will increase as long as the simulation is allowed to run. To determine a representative number, the damage parameter of each setup was measured at the same time. DYSMAS Post-Processor can display the damage as node or element based. When the "element face" option is on, the maximum damage

on the element is displayed and when the “contour face” option is on, the maximum damage on the node is displayed.

Figure 25 shows the damage parameter with the element face option while Figure 26 shows the damage parameter with the contour face option. Note that for these figures and all of the follow on simulations, the standoff distance is measured from the leading y-z face. The shockwave will first impact the y-z face meaning that the damage will typically occur on this face first.

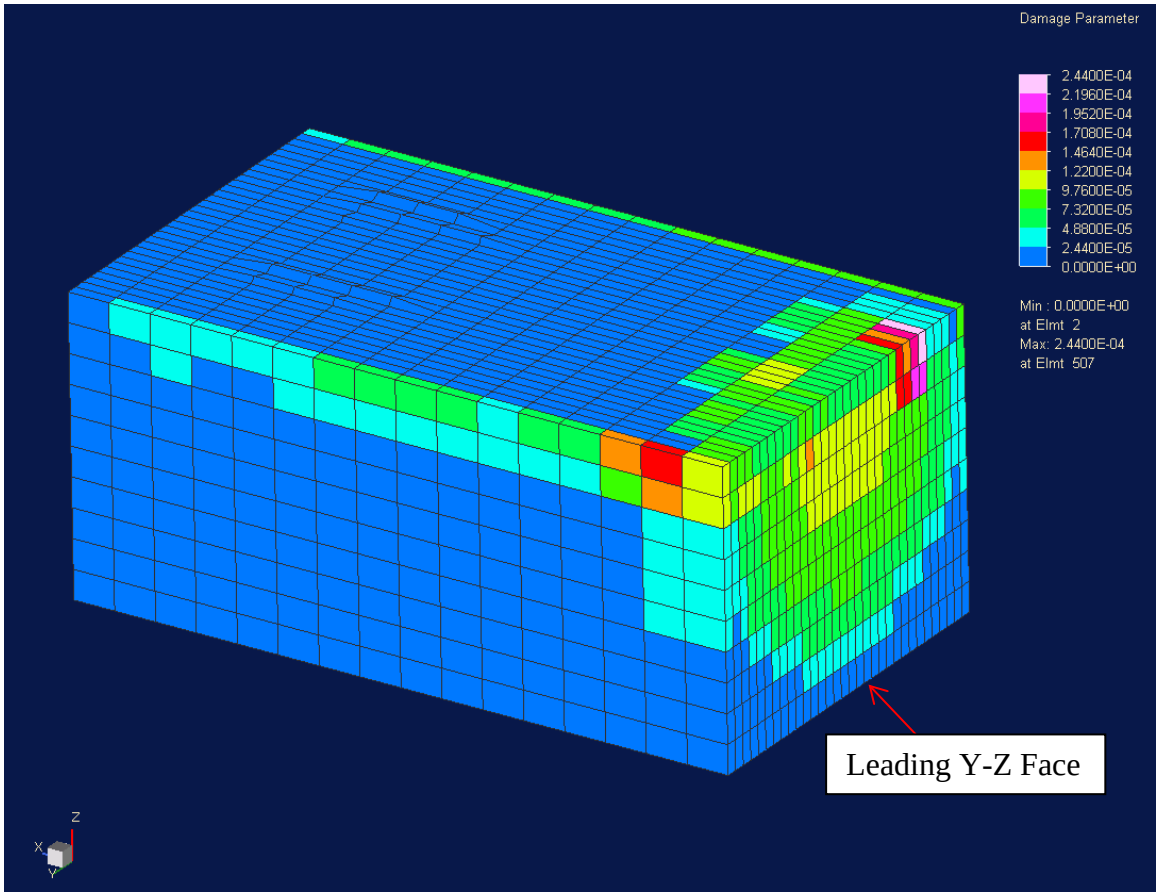

Figure 25. Element-based damage parameter for deep water when the bomb is detonated 3.66 m (12’) from the foundation.

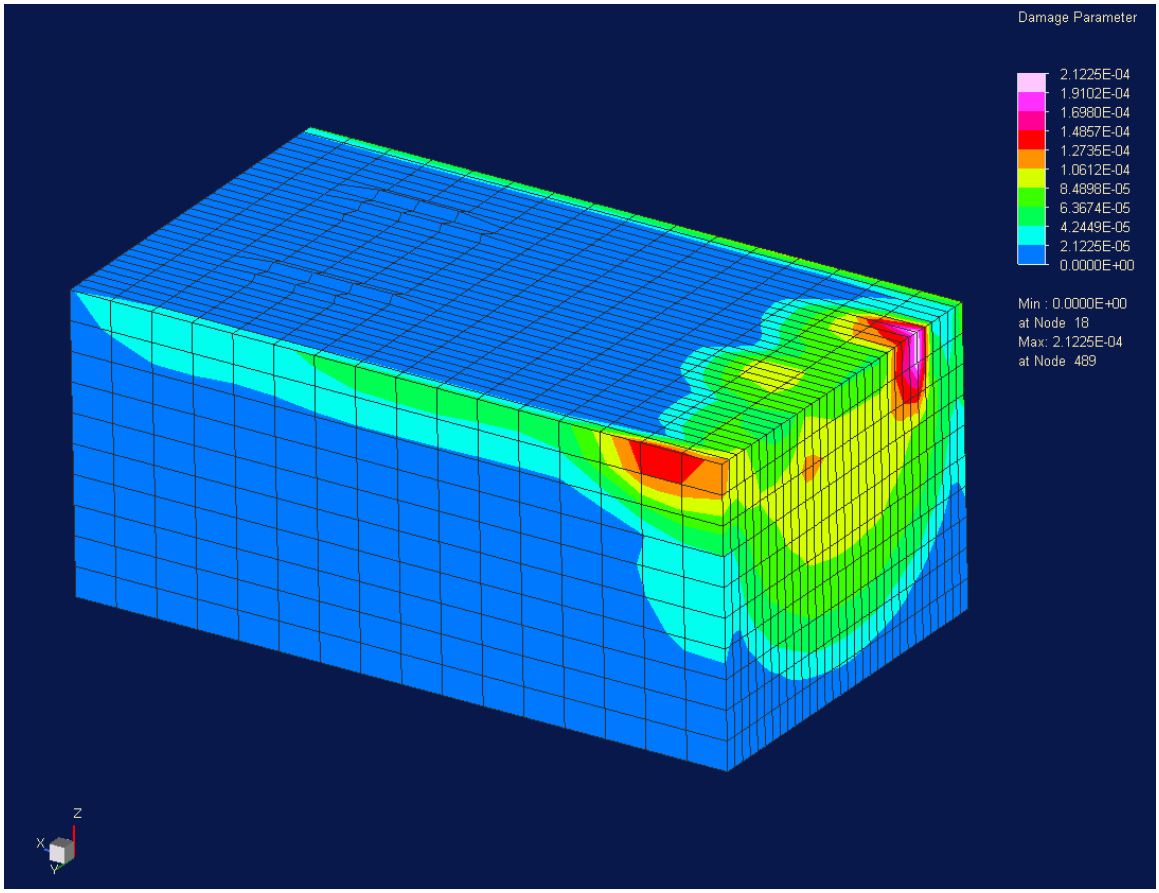

Figure 26. Nodal-based damage parameter for deep water when the bomb is detonated 3.66 m (12') from the foundation.

Although measured using two different parameters, the element and nodal based damage parameters demonstrated the same trends as seen in Figure 27 and Figure 28. That being said, element based data represents an average value across 4 distinct nodes, as opposed to only one [38]. Element based data will therefore be used in the rest of the data given. Please note that the simulations for the intermediate and deep water cases failed at the 30.48 m (100'). standoff distance and will not be used in this analysis. The cause of the failure will be the subject of future study.

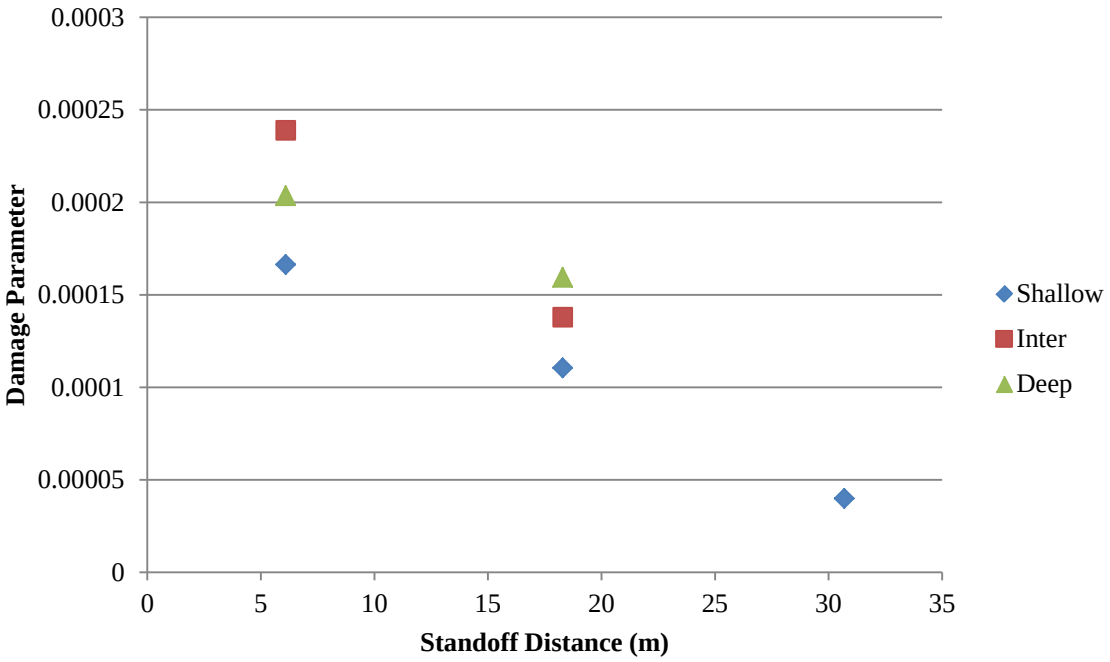

Figure 27. Element-based damage parameter at different depths and standoff distances

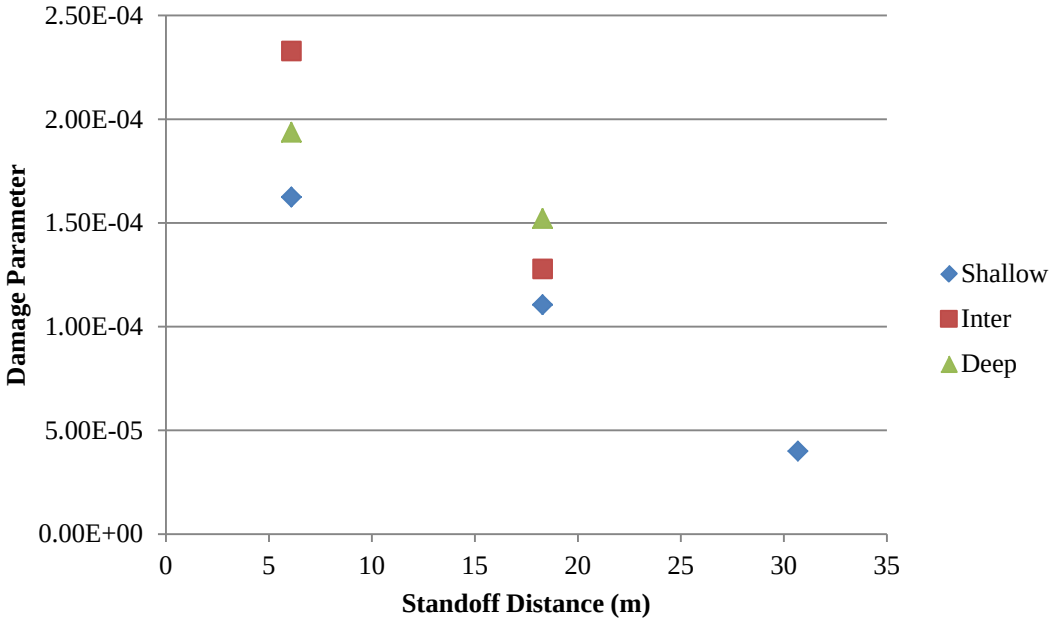

Figure 28. Nodal-based damage parameter at different depths and standoff distances

B. BOMB AT 12 FEET BELOW THE AIR-WATER INTERFACE

The data in Figure 27 and Figure 28 show the damage parameter of a bomb at 3.66 m (12') below the air water interface. The bomb will be targeting the same portion of the foundation because it is at the same standoff distance throughout this study. Figure 29 shows the test cases when the bomb is located 3.66 m (12') below the air-water interface. For the shallow case, the bomb is at the sand water interface, which is why the shallow water case consistently had less damage than the other two cases. The sand was able to absorb the impact of the bubble, meaning that the foundation received less pressure (Figure 28).

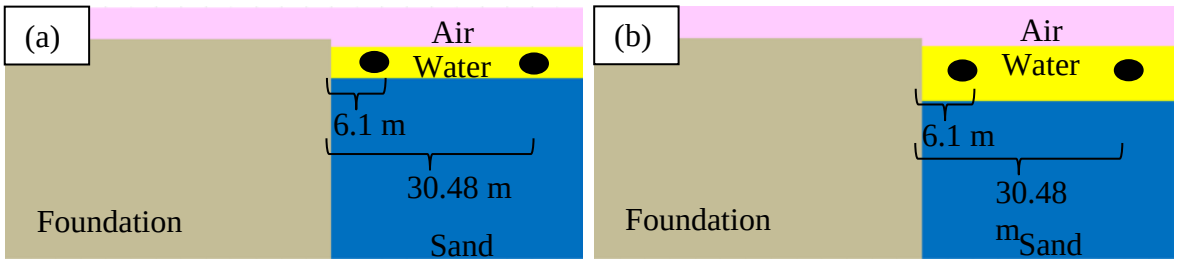

Figure 29. (a) the intermediate depth water, 10.36 m (34'), with the bomb at the near and far standoff distances (b) deep water, 16.46 m (54'), with the bomb at near and far standoff distances.

The deep water and intermediate depth cause the most damage at a 30.48 m (100') standoff and 6.1 m (20') standoff, respectively. To explain this trend, the location of the most damaged elements must be examined. Table 3 lists the most damaged element for each case while Figure 30 and 31 show the location of the most damaged element on the foundation.

Table 3. Most damaged elements at intermediate and deep water conditions when the TNT is detonated at a standoff of 6.1 m (20') and 30.48 m (100').

Depth	Standoff Distance	
	Near	Far
Inter	2030	1018
Deep	1006	1473

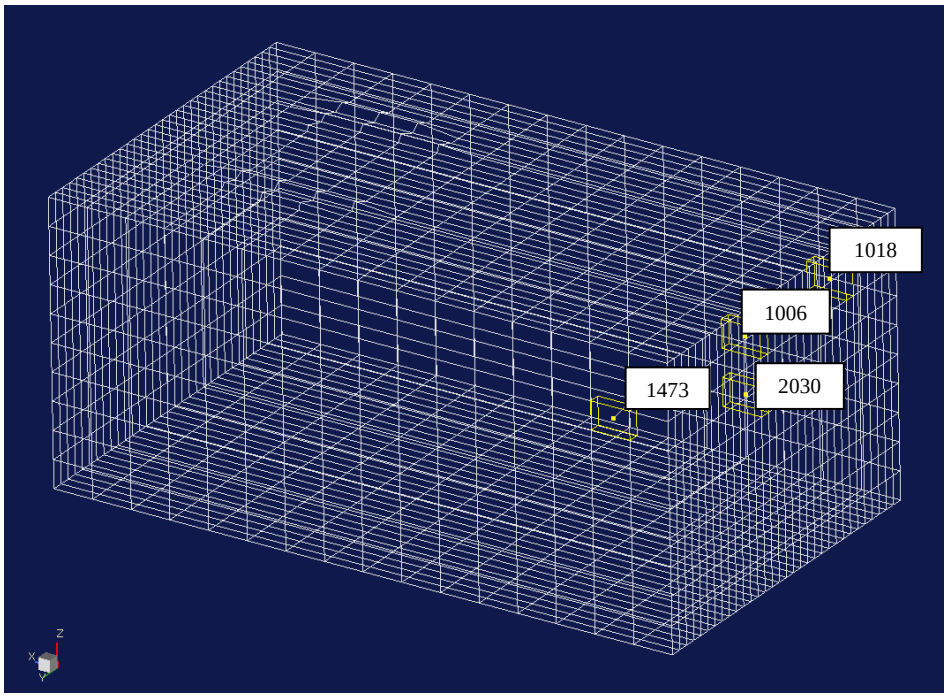

Figure 30. Isotropic view of most damaged elements in the foundation

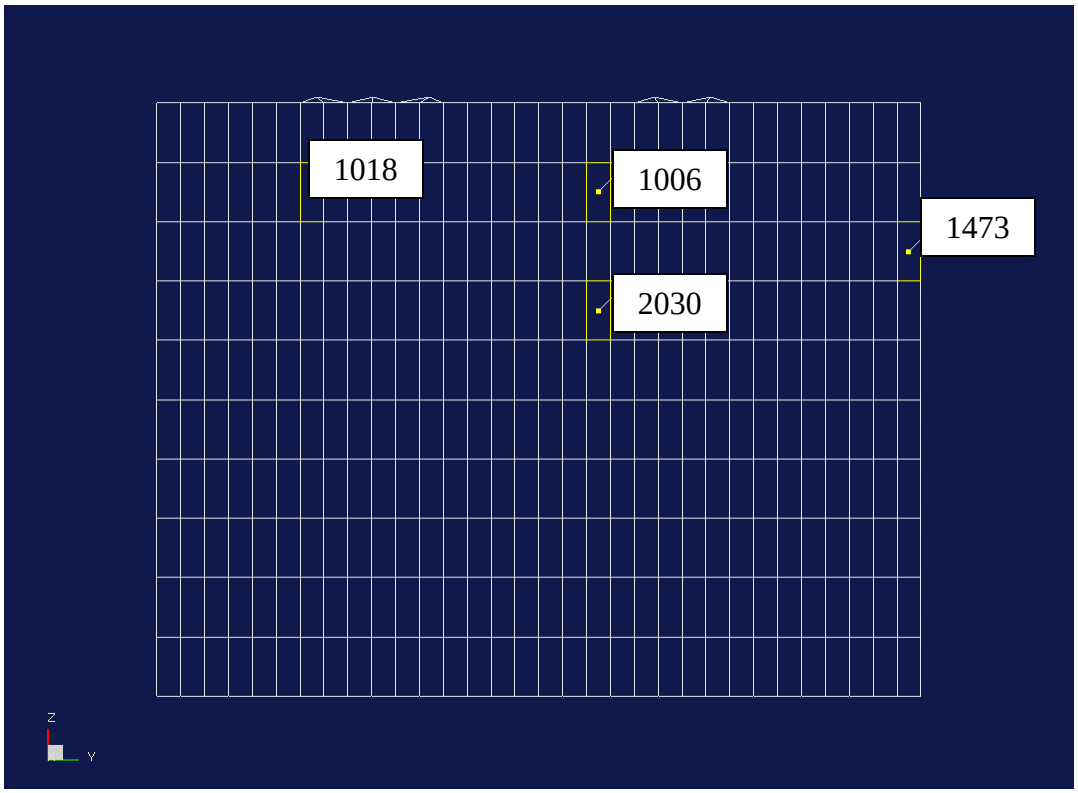

Figure 31. Most damaged elements on the front face of the foundation.

In the 30.48 m (100’) standoff case, element 1473 was the most damaged likely because it was located at one of the foundations corners, a geometrically weak spot. Because of the deeper water, the pressure bubble can expand to a greater radius without reflecting off the bottom or venting to the surface, causing the bubble to impact a greater portion of the foundation and subsequently hitting the corner. The intermediate depth and distance was allowed to expand more than if it were near the foundation, however, it was not able to expand as far as the deep water case because it vents to the surface much sooner. The further the detonation is from the foundation, the more energy the shockwave expends in migrating toward the structure. Consequently, the damage parameter is the least when the detonation is far from the foundation and increases, the closer the shockwave moves.

The intermediate depth for the closest standoff distance caused greater damage than the deep water because the strong bottom reflection. Figure 32 shows the damage for the deep water near case and one can see the center of the pressure wave from the initial shock on the front face of the structure. Note that the foundation is oriented so the top of the foundation, i.e., the air-water interface, is on the right, so the sand, water, and air are stacked from left to right. This indicates that the bubble has been allowed to expand and relieve some of the energy from the initial detonation.

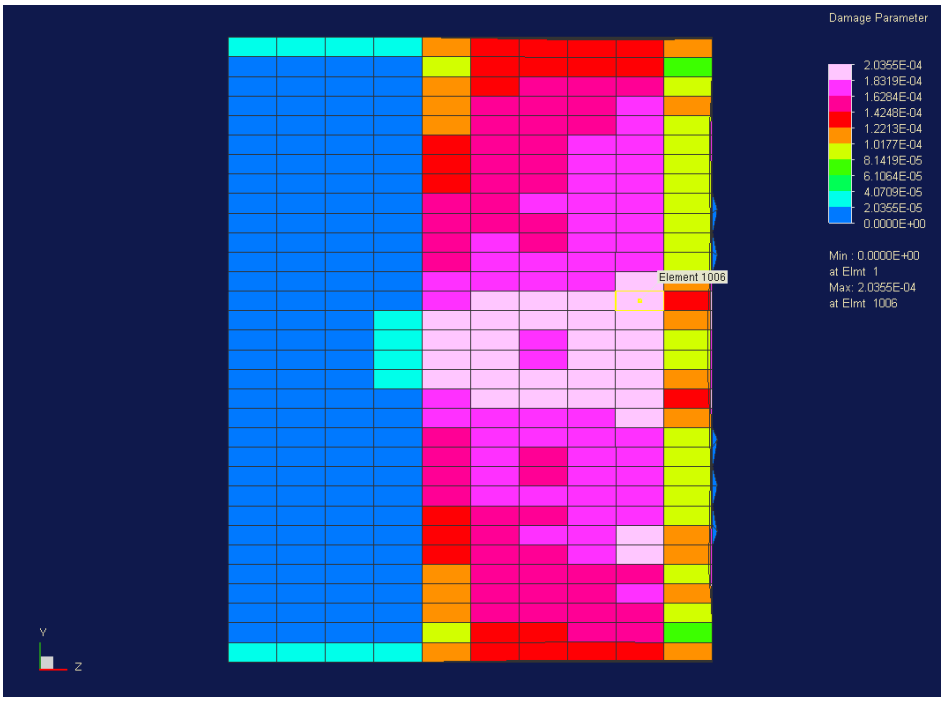

Figure 32. Damage parameter of the front face of the foundation in the deep water, 6.1 m (20') standoff distance scenario.

Figure 33 shows the damage for the intermediate case in which the bubble has not been allowed to fully expand because of the bottom interaction. The bubble is reflecting off the bottom and positively constructed with the shockwave, creating greater damage than if the bubble could expand unimpeded. Essentially, confining the bubble without allowing it to vent to the surfaced is increasing its damage on the structure.

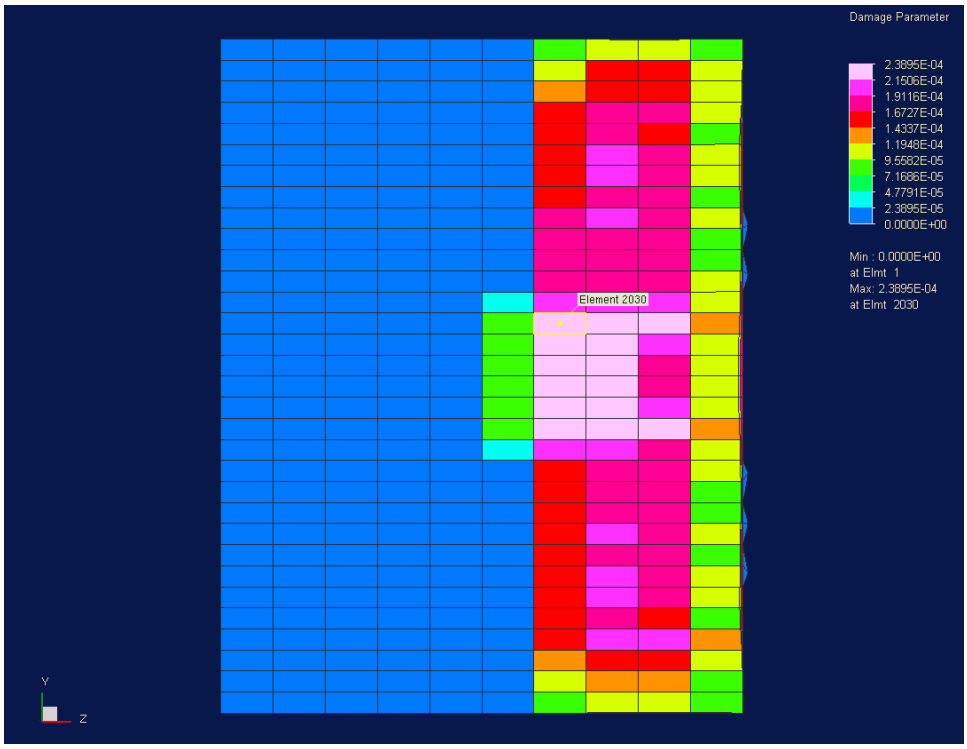

Figure 33. Damage parameter of the face of the foundation closest to the bomb in the intermediate water, 6.1 m (20') standoff scenario.

Further evidence of the strong constructive reflection is the pressure plots of the fluid. Figure 34 and Figure 35 show the deep and intermediate cases, respectively. Both cases have bottom reflection, however, the intermediate case is stronger than the deep case because the water column is approximately half as tall. The intermediate pressure wave therefore travels half the distance to reach the bottom and reflect back. It expends far less energy than the deep pressure wave traveling to the bottom and therefore the reflection is much stronger. The shorter distance also causes the reflection to occur much earlier in the intermediate case. The initial shockwave is still loading the structure as the bottom reflection interacts with the structure, causing greater damage. The comparative strength of reflection and shorter time of reflection increases the damage done to the structure in the intermediate depth cases.

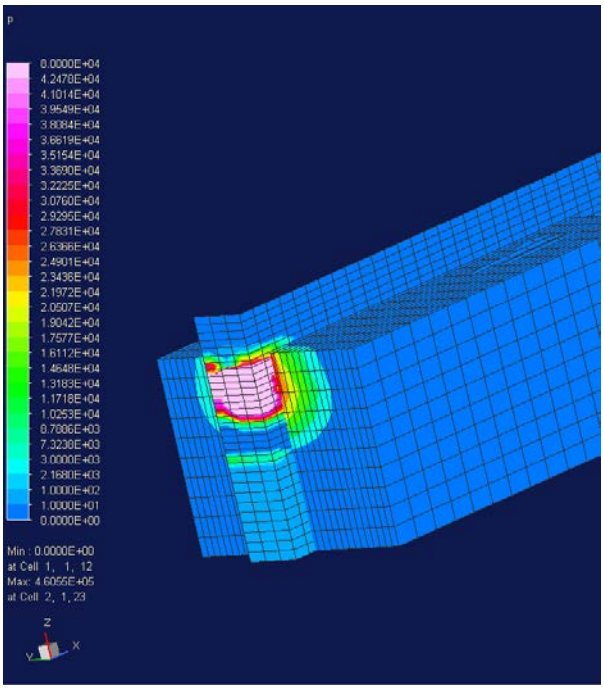

Figure 34. Deep water case at 889E-3 ms.

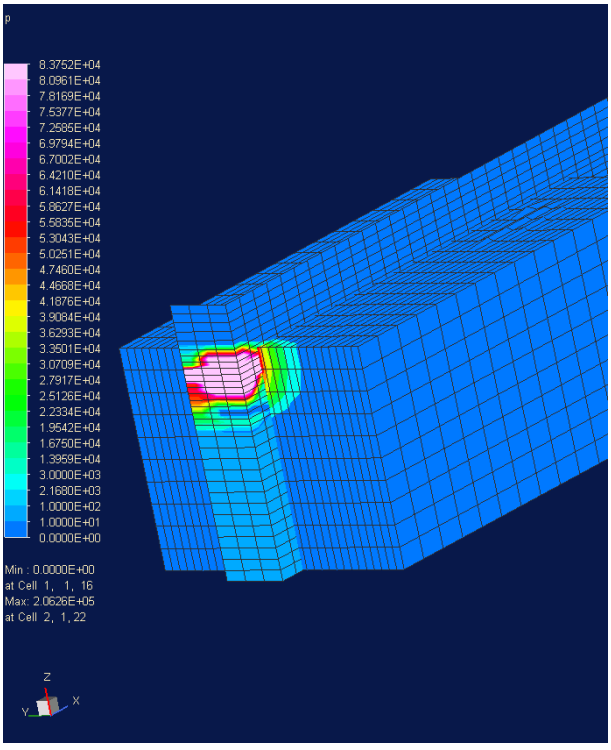

Figure 35. Intermediate depth case at 462E-3 ms.

C. BOMB AT SAND-WATER INTERFACE

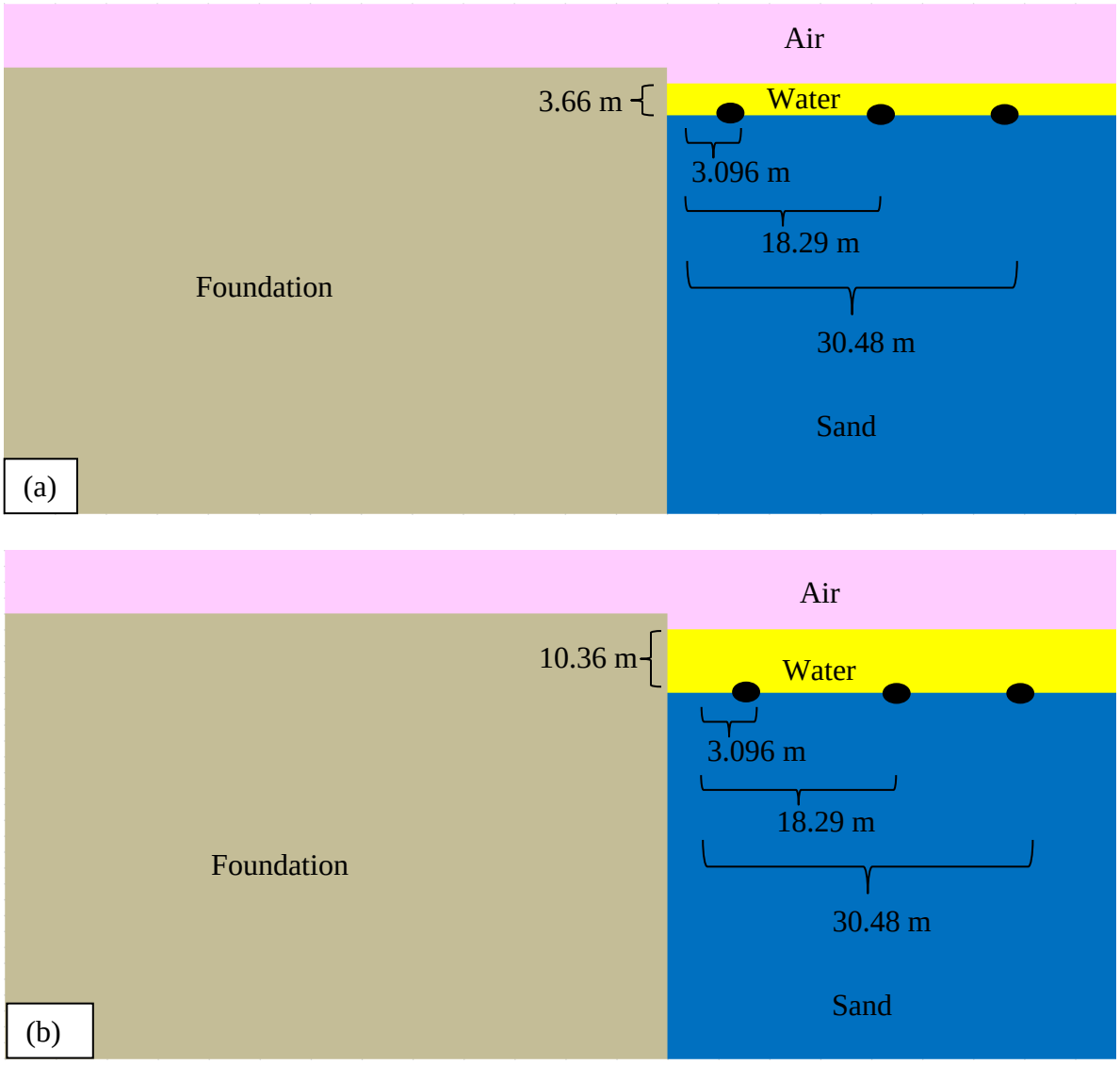

Figure 36. The image illustrates the following: (a) bomb at sand water interface in shallow water, (b) bomb at sand water interface in intermediate water, and (c) bomb at sand water interface in deep water. (Image c is on the following page.)

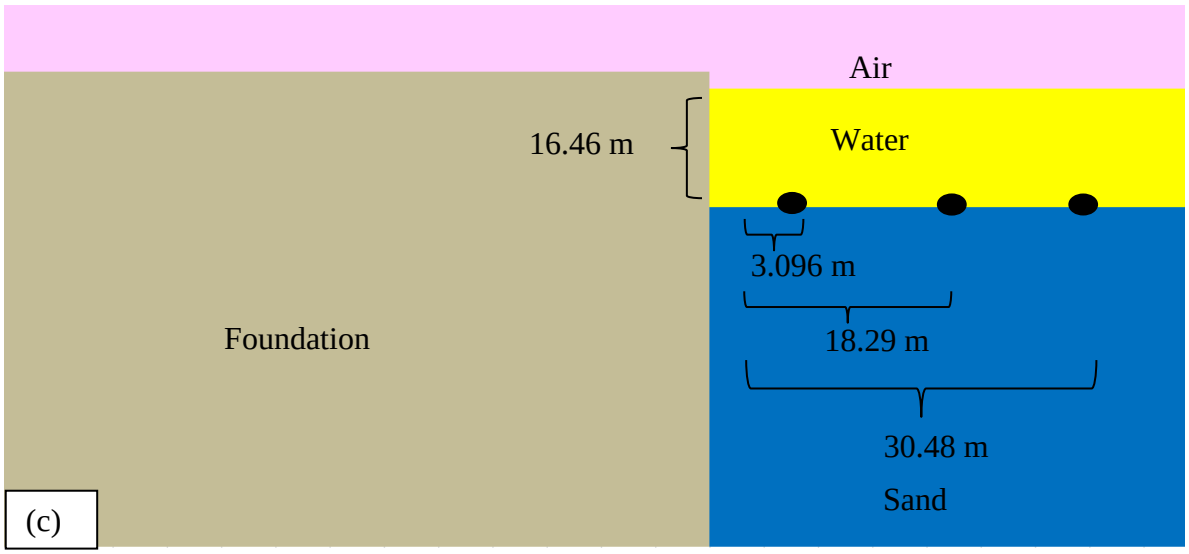

Figure 36 (c) continued from previous page.

This phase of the depth study consisted of placing the bomb at the sand water interface and detonating at the shallow, intermediate and deep depths and near, intermediate, and far horizontal standoff distances (Figure 36). When executing a controlled detonation of an underwater IED, EOD units will sink the bomb to the ocean floor. This study is directly aimed at this scenario and will examine if and how water depth impacts the effect of the bomb on nearby infrastructure. For this study, the damage parameter was analyzed at 22.7 ms for all of the given scenarios. This time step was chosen because the deformation in the foundation was too large for the results to be reliable after 22.7 ms.

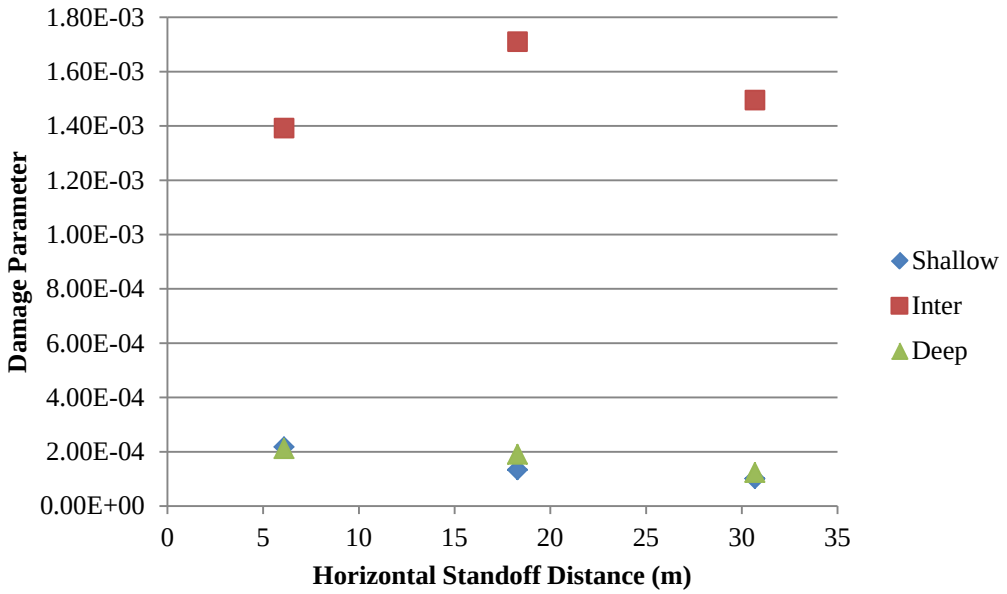

Figure 37. Damage parameter when the bomb is located at the sand-water interface.

The intermediate depth caused the greatest damage to the structure by a factor of ten as seen in Figure 37. Looking at the development of the damage over the course of the simulation can provide insight into these results. The following three figures show the shallow, Figure 38, intermediate, Figure 39, and deep depths, Figure 40, 17.3 ms after the bomb is discharged 30.48 m (100') from the foundation. The elements with the most damage at 22.7 ms are highlighted.

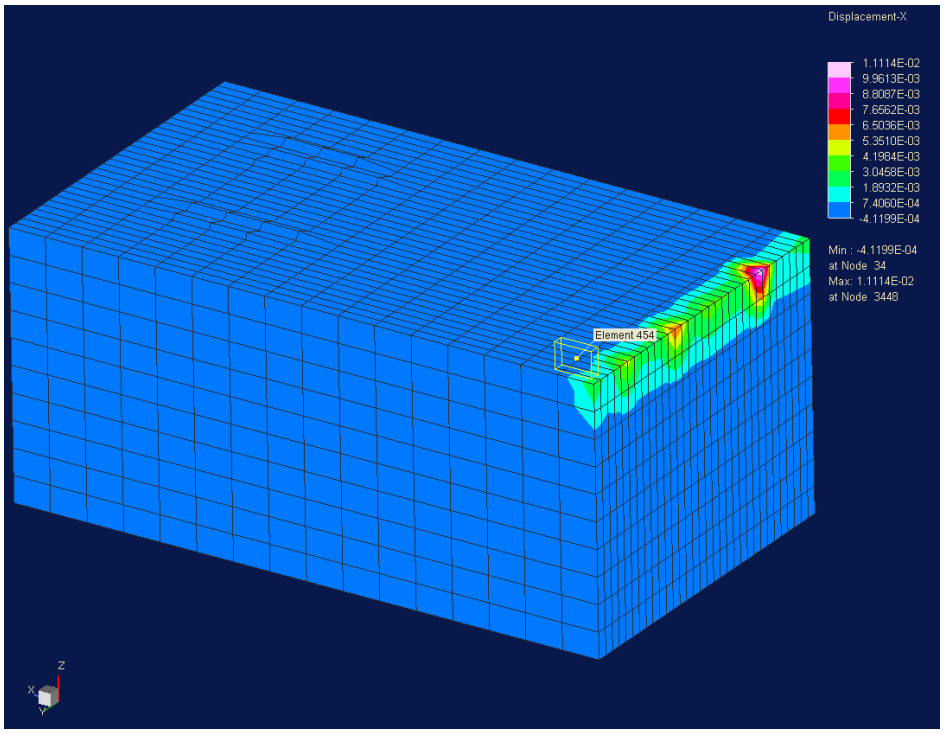

Figure 38. Shallow water detonation of a bomb 30.48 m (100') from the foundation.

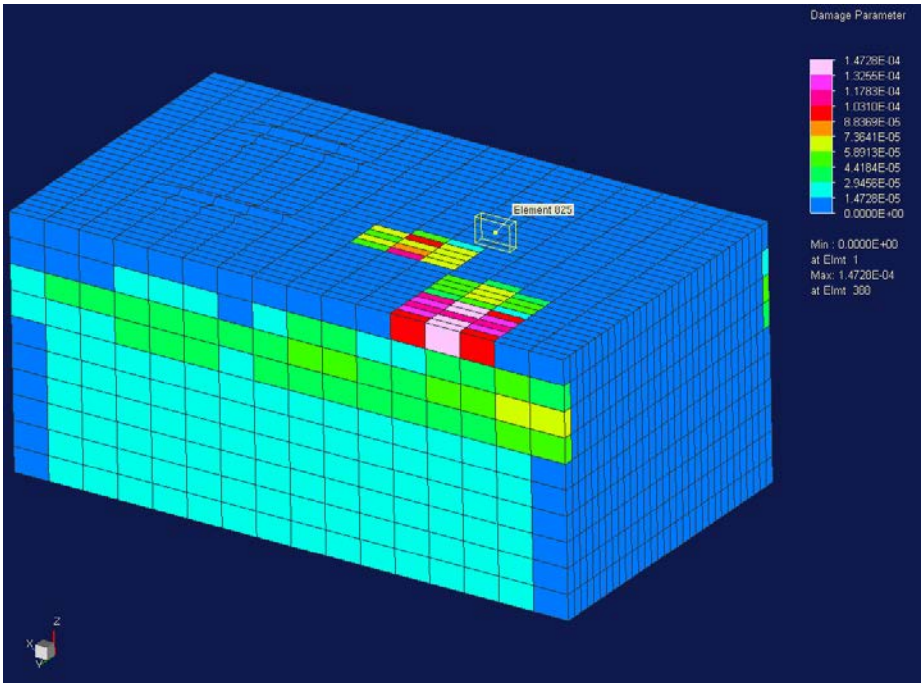

Figure 39. Intermediate depth detonation of a bomb 30.48 m (100') from the foundation.

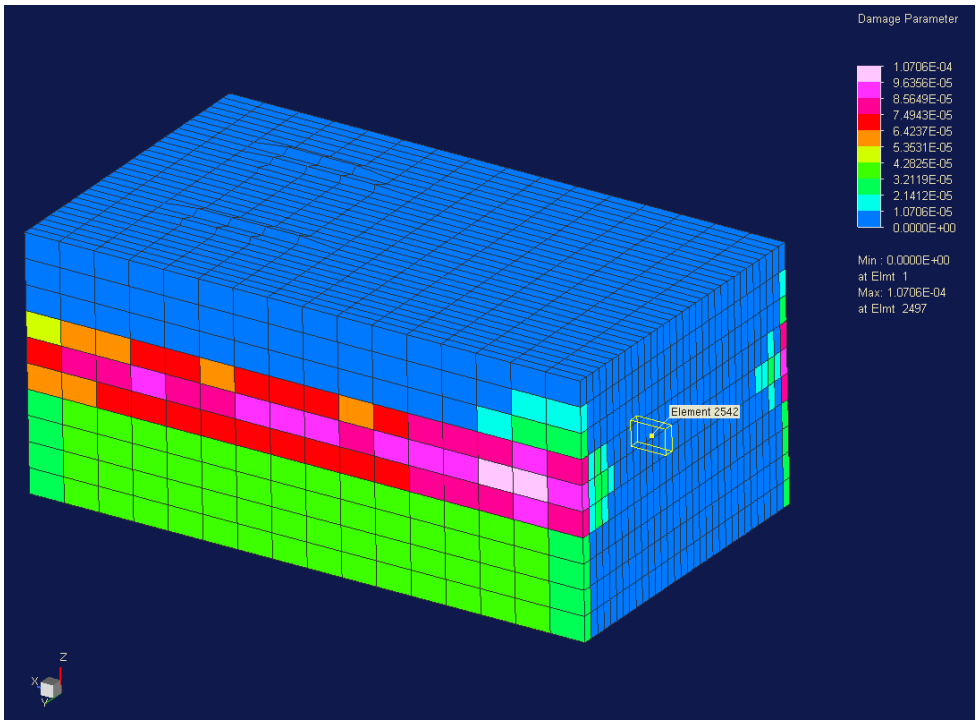

Figure 40. Deep water detonation of a bomb 30.48 m (100') from the foundation.

In the shallow water case, the shockwave only impacts the top, leading edge of the foundation. The pressure front is slowly rising as it migrates toward the foundation making it vent to the surface much sooner, loose energy, and cause less damage. Because it physically impacts the foundation the least out of all three cases, it causes the least damage. If the detonation is very close to the foundation, the pressure will not have the space to migrate to the surface. The full pressure force will be felt by the foundation. These observations are the driving force behind the shallow water case causing less damage than the deep water case at intermediate and far standoff distances. They also provide insight into why the shallow water case causes more damage than deep water when the detonation is close to the foundation.

The intermediate depth causes the most damage to the foundation because the shock wave impacts the top and side of the foundation. As stated earlier, the foundations' corners represent the weakest locations, so the more corners the front impacts, the more damage it will cause. The pressure pushes around the side of the foundation and over the

top, damaging more surfaces than either the shallow or deep water. The intermediate distance caused the most damage out of the tested standoff distances. The difference between all the intermediate depth damages is less than 3E-4. This delta is tiny enough to be considered negligible considering the difference between the intermediate distance cases and other distances.

The deep water case generates relatively little damage because the shockwave only impacts the side faces of the foundation. The detonation location is deeper therefore the front requires more time to migrate to the surface and the top of the foundation. As seen in Figure 39 the damage is concentrated on the side and will eventually migrate to the front face as the concrete crumbles. The deep water also means that there is a greater hydrostatic pressure acting on the bomb as it detonates, causing the explosion to expend more energy as it expands. In this sense, the water acts as a stifling measure against the impact of the bomb.

THIS PAGE INTENTIONALLY LEFT BLANK

VII. SENSITIVITY STUDY RESULTS

To determine the impact of the loading conditions, orientation and volume fraction of reinforcement, the maximum damage on the foundation was recorded and compared. These parametric studies will focus on the applicability of building a high fidelity model. If, for example, the foundation's damage shows little response to changes in the load, this model can be applied to a wide range of loading conditions. If the model is very load sensitive, then it can only be applied to a narrow range of scenarios. The same can be said for the orientation of the reinforcement as well as the volume fraction.

A. LOAD SENSITIVITY

Five different loads were applied to the foundation with a volume fraction of 0.35 to determine how sensitive the damage parameter is to changes in the load: 11.34×10^6 kg (25 million pounds), 34.02×10^6 kg (75 million pounds), 45.36×10^6 kg (100 million pounds), 73.48×10^6 kg (162 million pounds), 90.72×10^6 kg (200 million pounds). These loads were applied as pressure loads, meaning that the load was divided between the selected elements on the exterior of the foundation. This range of loading was selected because it represents an expected loading range on a suspension bridge. Figure 41 shows the location of the pressure load on the top of the foundation. These locations were chosen because they represent where the pedestals would be located and where the superstructure's load would be applied.

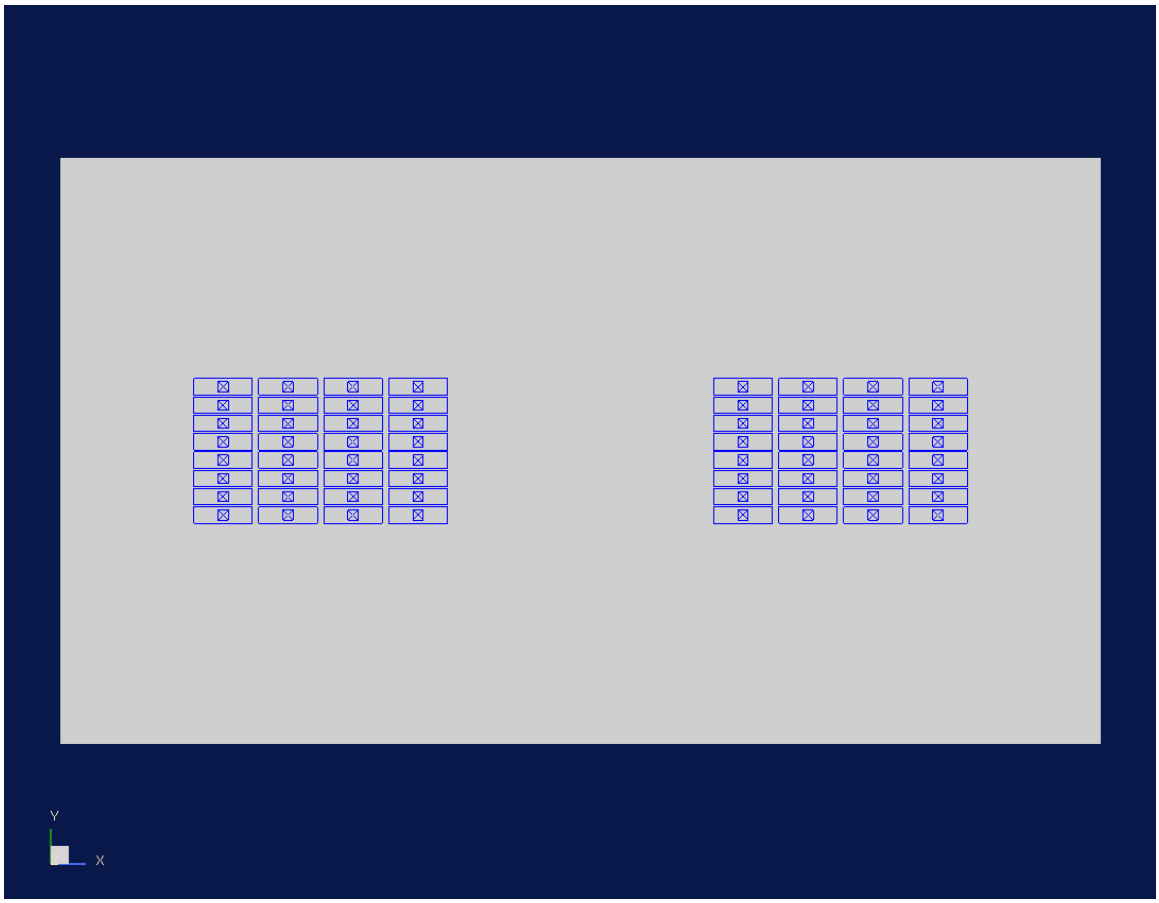

Figure 41. Top-down view of the pressure load applied to the foundation.

The bottom of the foundation was fixed to ensure that the additional load did not force the foundation out of the DYSMAS environment. When the foundation was not fixed, it was pushed into the porous sand causing the pores to collapse. The interior pressure of the sand would drop to zero, leading the model to fail from pressure equilibrium error. Each of the bottom nodes was fixed in 6 degrees of freedom meaning no rotation or translation was permitted.

The greatest damage to a single element was recorded 6.475 ms after the detonation of a 49.99 kg (108 lb.) TNT bomb when the bomb was located at the sand-water interface in 16.46 m (54 ft.) of water. A smaller bomb was used for this study to ensure that the foundation would not fail thereby cutting off analysis of the damage

parameter. There was a linear response between the increased load and the damage parameter as seen in Figure 42.

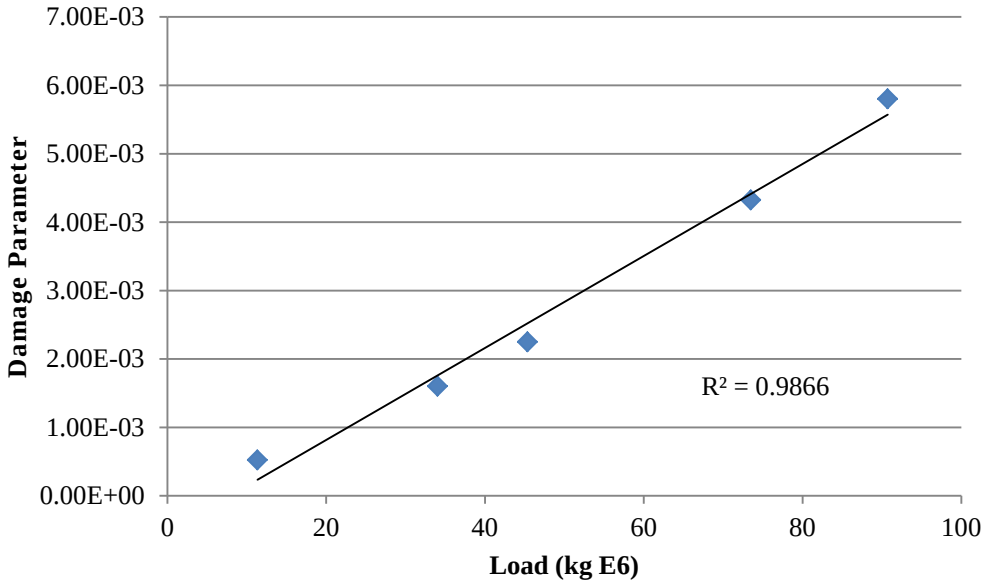

Figure 42. Damage parameter response to variable load in a 0.35 reinforcement volume fraction concrete foundation.

Based on the data, when the load is increased by one million pounds, the damage parameter will increase by 3E-5. This is a relatively small increase in damage relative to a large change in loading. As such, this foundation can be used to analyze damage for a wide range of loading conditions.

Although the greatest damage to an element is not responsive to changes in load, the change in load does make a difference to the whole system. Figure 43 and Figure 44 show the distribution of damage to the foundation in two separate loading cases. For the heavier load, the damage to the area under the pedestal is greater than the lighter case. Because the pedestal covers a large area of the top of the foundation, this incremental change in damage is not insignificant.

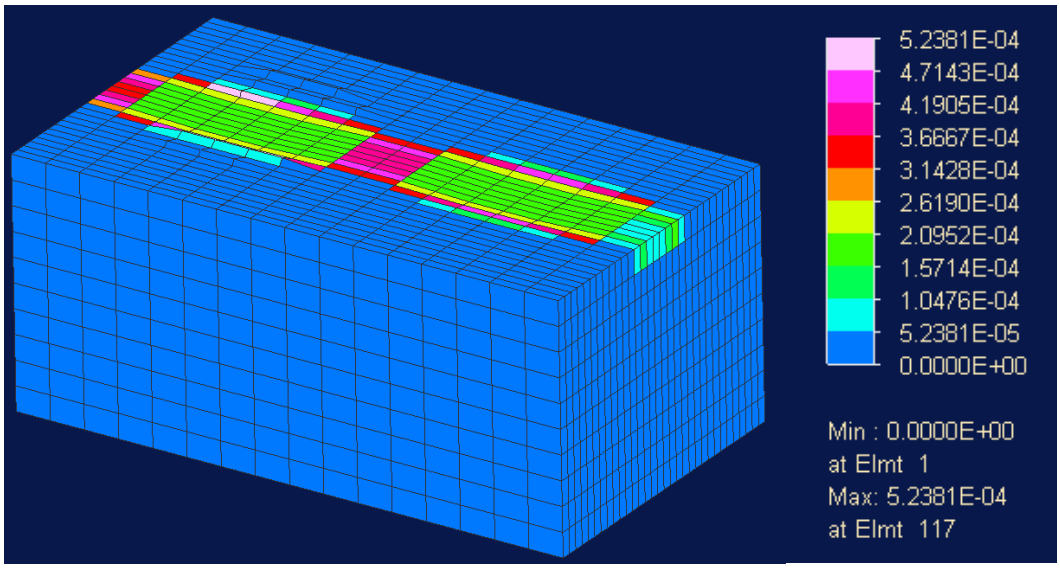

Figure 43. Distribution of damage for the 11.34 x 10^6 kg (25 million pounds) load.

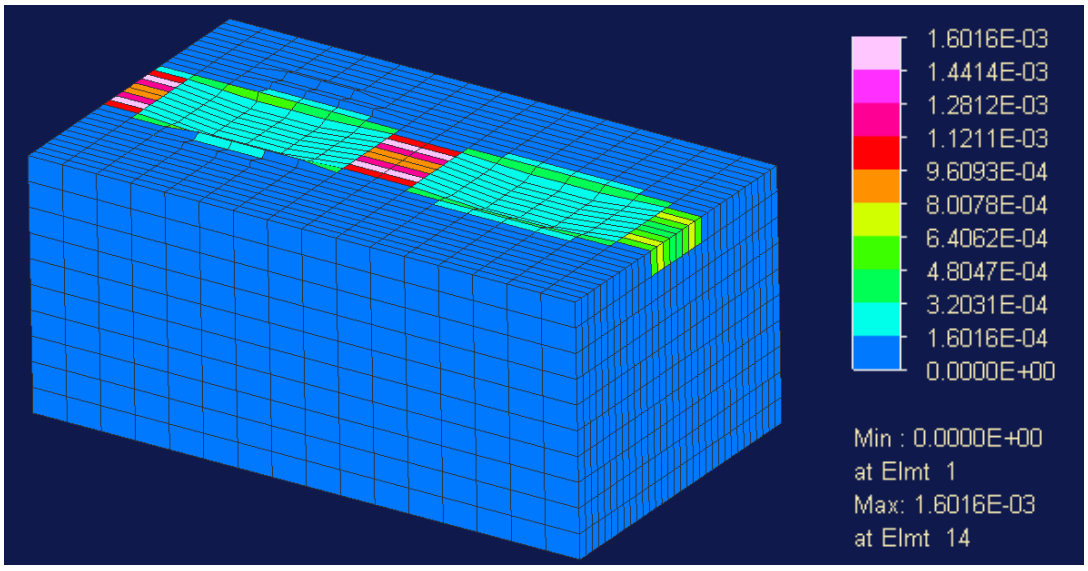

Figure 44. Distribution of damage for a 34.02 x 10^6 kg (75 million pounds) load.

B. ORIENTATION

The importance of the orientation of the rebar was studied by placing all of the rebar in the model in the x-, y-, or z-direction. The 195 kg (430 lb.) TNT was then detonated at the sand-water interface in 16.46 m (54 ft.) of water and the damages compared at 9.75 ms. Figure 45 shows the orientation of the foundation relative to the shock wave. The y-z planar face will receive the direct impact of the shockwave.

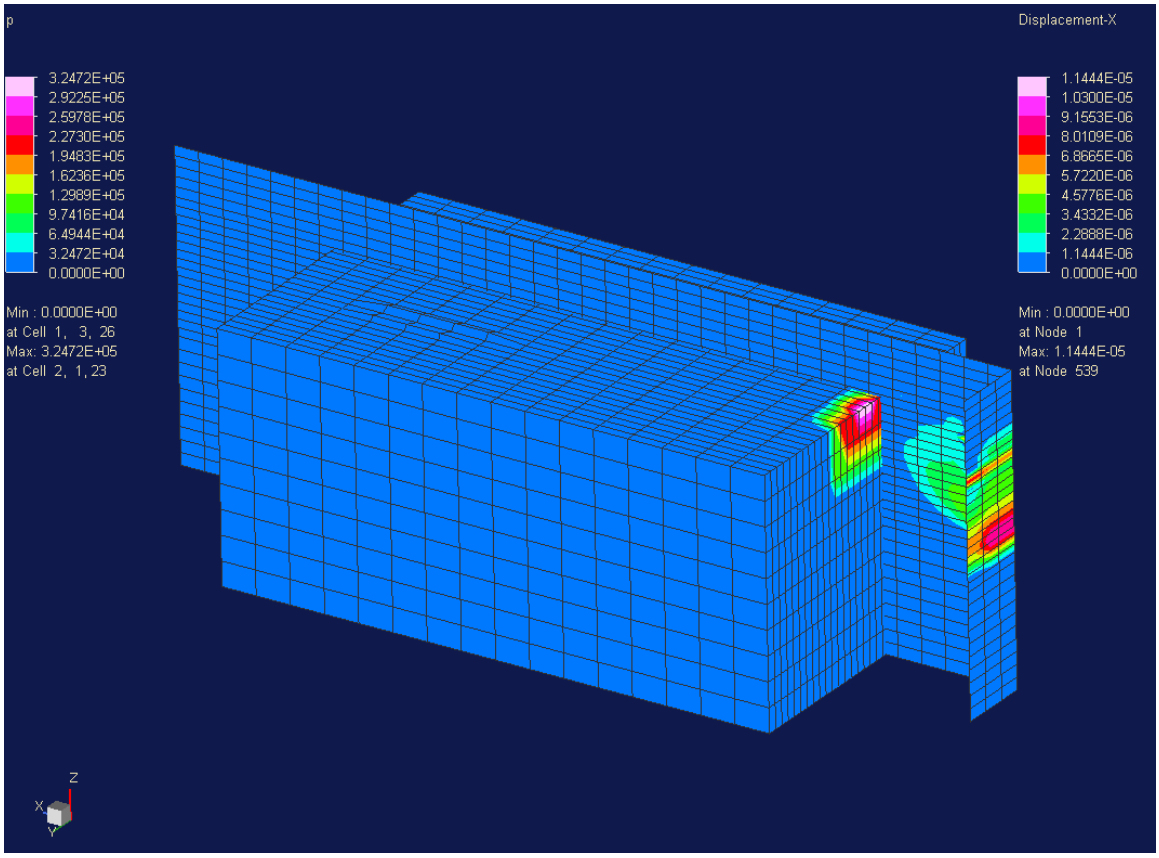

Figure 45. Orientation of foundation relative to the detonation.

Because the y-z plane is perpendicular to the motion of the shockwave, having reinforcement in those directions is vital to the foundations' survivability. When there was only reinforcement in the x-direction the damage parameter was much greater than in the y- or z- directions. The damage parameter in the y- and z-directions is very close,

however, the z-direction had slightly less damage (Table 4). All the z-directional reinforcement was part of the foundation that was buried in the sand. The added mass of the sand kept the rebar more stable as the shockwave moved over the foundation and kept the concrete from shearing off the rebar.

Table 4. Damage parameters in three different global orientations.

Orientation	Damage Parameter
X	1.0980E-04
Y	1.0284E-04
Z	1.0224E-04

C. REINFORCEMENT SENSITIVITY

A loaded foundation with varying reinforcement volume fractions was run through the UNDEX simulation to understand the importance of accurately modeled reinforcement. The reinforcement was oriented so that 60% was in the z-direction and 20% was in the x- and y-directions, respectively. The model from the loading study was used for this parametric study with a 45.36 x 10^6 kg (100 million pounds) loading conditions and fixed bottom. The 49.99 kg (108 lb.) TNT bomb was also used for this simulation.

As the reinforcement volume fraction increases in all dimensions, the damage parameter decreases at varying rates. Figure 46 shows that as the foundation takes on characteristics of steel rebar, it is less prone to damage. Note that the damage parameter has been multiplied by a factor of 1000 to better view the results. The relationship between the damage and the volume fraction is negatively linear and for this time step, 9.6 ms, has a slope of -0.0016. This slope indicates that there is a very low response in the damage parameter as the volume fraction is varied.

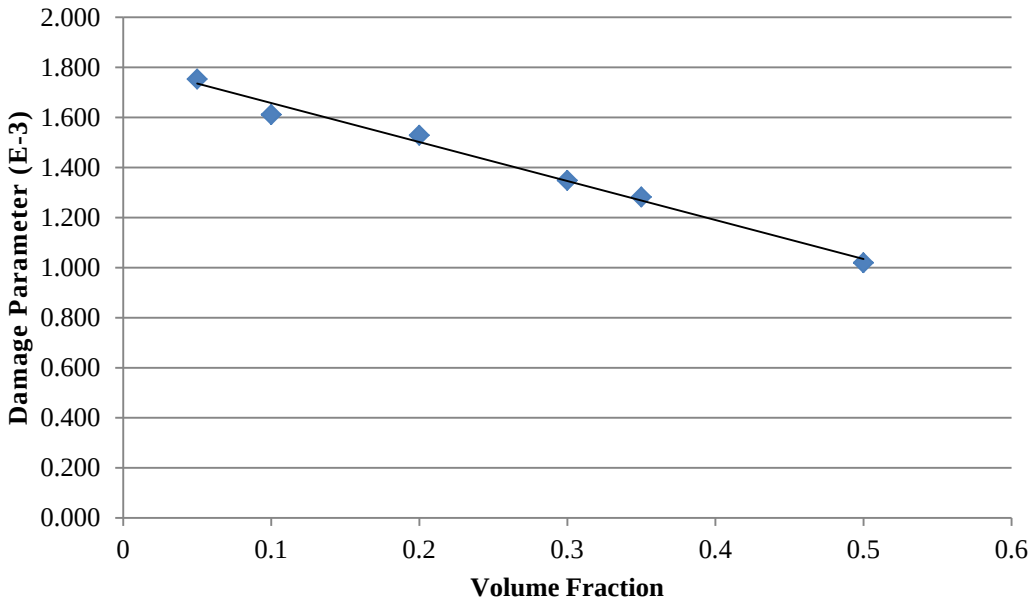

Figure 46. Damage parameter at a given volume fraction at 9.6 ms.

As the simulation was run for a longer time, the damage parameter showed increased response to changes in the level of reinforcement. Figure 47 plots the slope of the damage parameter versus volume fraction at different time steps in the simulation. As concrete crumbles, the reinforcement will continue to stand and allow the foundation to support the load of the superstructure. Concrete will begin crumbling as soon as it experiences the pressure from the underwater explosion and continue to crumble after the bubble has moved over the foundation. As such, the reinforcements' ability to withstand the force of the shockwave becomes more apparent as the concrete continues to fail over time. Essentially the reinforcement is not critical immediately after detonation, but becomes more critical as the scenario progresses. In short-term modeling, the reinforcement does not need to be perfectly modeled, but for longer simulation runs, the reinforcement should have a high precision volume fraction.

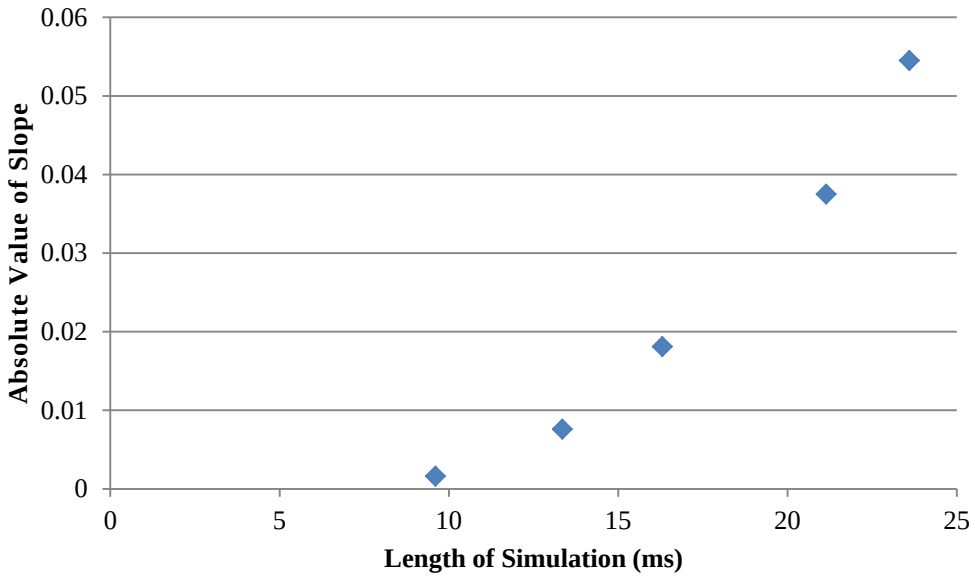

Figure 47. Absolute value of the slope, which indicated the relationship between damage parameter and volume fraction, and the length of the simulation.

Eventually the damage parameter reached an asymptote at 203 ms. Figure 48 shows the progression of the damage parameter of a 0.5 and 0.55 reinforcement volume fraction foundation. The damage parameter increases rapidly between 74.1 and 80.7 as the initial shockwave passes over the foundation. The damage momentarily converges then begins to increase again as the concrete starts to crumble. When the stress drops below the initial yield surface, the plastic flow of the failure will halt. When the failure stops propagating, the damage parameter reaches a limit, signaling the end of the trauma to the foundation.

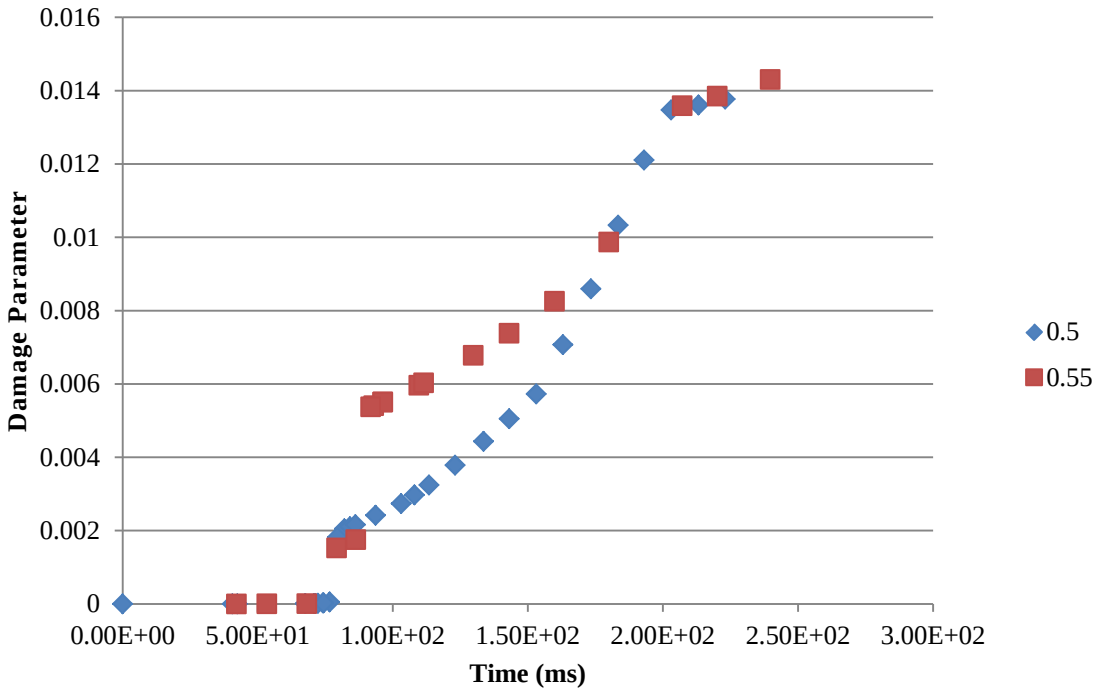

Figure 48. Damage parameter progression for 0.5and 0.55 reinforcement volume fraction foundation.

Although the maximum damage to an element is somewhat comparable, the distribution of damage is very different depending on the volume fraction. Figure 49 and Figure 50 show the distribution of damage to a 0.1 and 0.35 reinforcement volume fraction respectively at 12 ms. Although this is still considered a “short” simulation and the damage should not be highly dependent on the volume fraction, the area of maximum damage is much greater for the 0.1 reinforcement than the 0.35. This trend holds true for all of the volume fraction values tested meaning that models should have a high fidelity representation of the volume fraction.

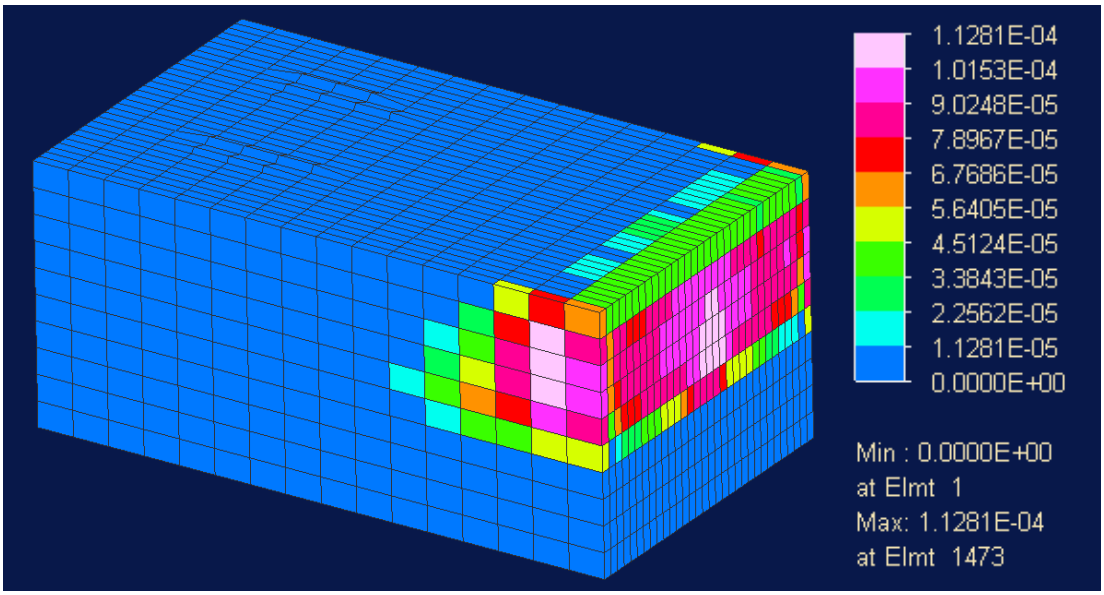

Figure 49. Damage to 0.1 reinforcement volume fraction concrete foundation.

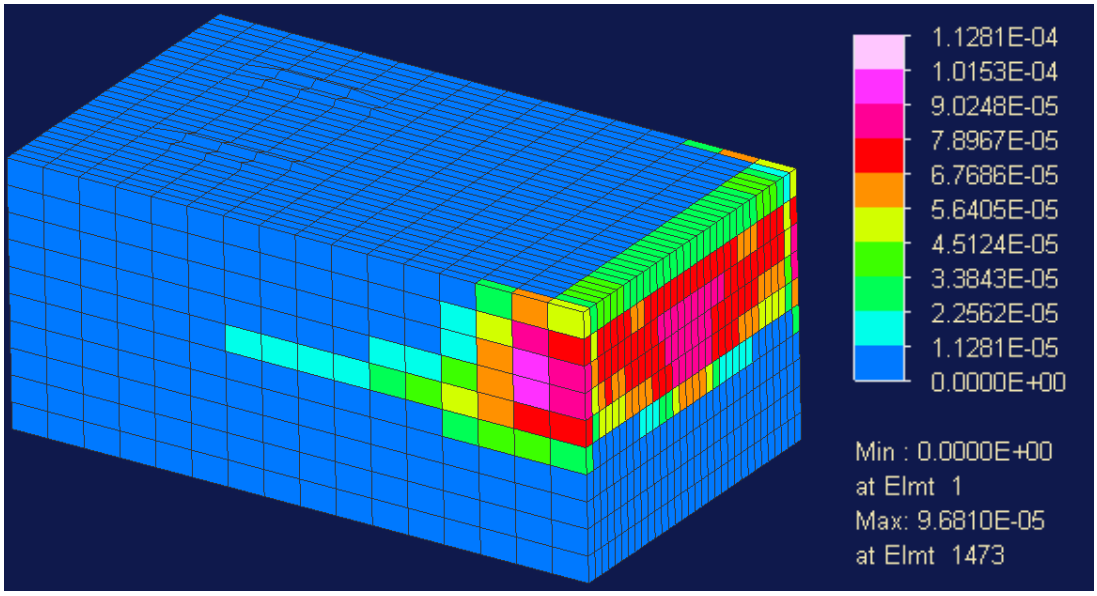

Figure 50. Damage to 0.35 reinforcement volume fraction concrete foundation.

VIII. FINAL REMARKS

A. CONCLUSION

A series of simulations were conducted to characterize the behavior of bridge foundations in response to underwater explosions. Initially, a concrete bridge foundation based on actual bridge dimensions was tested at varying water depths and horizontal standoff distances to determine the most critical scenario. The first parametric study varied the water depth and standoff distance of the environment when a TNT bomb is placed at a depth of 3.66 m (12 ft.). Out of a test matrix ranging from shallow to deep water and near to far standoff distance, an intermediate water depth and near standoff distance created the most damage on the particular bridge foundation model that was studied. A strong bottom reflection of the shockwave at the intermediate depth caused the foundation to experience the greatest force and subsequently undergo the most damage. The closest standoff distance placed the foundation closer to the detonation meaning that the shockwave had to expend less energy traveling through the water and therefore had more energy when it contacted the foundation.

The second parametric study again varied the water depth and standoff distance, but this simulation placed the TNT bomb at the sand-water interface. Again, the intermediate depth caused the greatest damage by a factor of ten, but this simulation showed that the intermediate distance, 10.36 m (34 ft.), caused slightly more damage than the near and far distances. The difference in damage for the intermediate cases was less than 3E-4 and is considered a negligible difference given the difference in damage between the intermediate depth and other depths. As stated earlier, intermediate depths allow for constructive interference of the shockwave from bottom reflection causing significantly more damage than the other cases. Subsequently, EOD units should aim to detonate bombs in either very shallow or very deep water to aid in the bridge's survivability. To further guarantee the bridge's safety, the unit should try to take the bomb as far from the foundation as possible.

The same generic foundation was used in three sensitivity studies that focused on the parameters necessary for a high fidelity model. The first study focused on load sensitivity and showed the damage parameter is very insensitive to changes in the load. Essentially, a model with a given load can be used to model a similar foundation with a very different load. The second study examined the criticality of properly modeling the orientation of the reinforcement. The z-direction reinforcement is the most important to the structure and is therefore the most important to accurately model. The final sensitivity study explored how the damage parameter responded to changes in the reinforcement volume fraction. For short simulations, less than 10 ms, the damage parameter does not vary greatly with changes in the volume fraction; however, as the simulation time is extended, the volume fraction impacts the damage parameter more and more. Eventually the damage parameter will reach a limit, however, the limit cannot be known until the simulation is allowed to run for an extended time. Accurately modeling the reinforcement of a foundation is therefore critical to capturing its response to an UNDEX.

Knowing which parameters have the most impact on modeling a bridge is crucial in the application of survivability studies. Although there is a wide range of bridge superstructures, bridge foundations are all very similar. There does not need to be one foundation survivability study for every bridge. This thesis explores the aspects of foundations that enable future studies to apply their results to foundations outside of the one they have specifically modeled. If an IED were to be placed by a bridge that has not been studying for its survivability, EOD units would be able to employ data from another foundation in its group to better ensure the bridge's safety and security. By understanding that reinforcement needs to be accurately modeled and loading can vary, future engineers and EOD units can better understand how each bridge will fail, preserving the safety and security of the country.

B. FURTHER STUDIES

Port security in cities throughout the United States has been and will continue to remain a national economic issue. As such, the survivability of the various bridges is a subject of continual future work. Modeling each bridge and understanding how each

bridge will react to a wide range of detonations and distances will enhance security measures throughout the country. The first step in this process would be to group bridges based on the critical parameters of their foundations. Because the superstructure can be simply modeled as a load onto the pedestals, the construction of the superstructure is irrelevant to these studies. These models and the subsequent findings can be used to map a table of approximate damage potential at a current location and charge weight. Ultimately, unit commanders called on scene to safely detonate the bomb can use these tables to ensure the survivability of every structure throughout the United States.

THIS PAGE INTENTIONALLY LEFT BLANK

APPENDIX A. MATERIAL INPUTS

A. AIR

```
format=00002

<OPTIONS>
  title="gamma law equation of state"
  eosType=g_law
<END OPTIONS>

<REFERENCE>
  rhoRef=.00075
  eiRef=9.6154e+8
  cRef=1.64e+4
<END REFERENCE>

<LIMITS>
  rhoMin=1.d-06
  eiMin=1.d-4
  pMin=2116.8
<END LIMITS>

<EOS VARS>
  gamma=1.4
<END EOS VARS>
```

B. WATER

```
format=00002

<OPTIONS>
  title="tillotson water model"
  eosType=till
<END OPTIONS>

<REFERENCE>
  rhoRef=1.0
  eiRef=3.5420001e+09
  cRef=147600.0
<END REFERENCE>

<LIMITS>
  rhoMin=9.9999998e-03
  eiMin=-9.9999998e+10
  pMin=50000.0
<END LIMITS>

<EOS VARS>
  omega=.28000000119
  rho0=1.0
  ei0=3.5420001e+09
  p0=1.e+06
  A=2.2000001e+10
  B=9.5400002e+10
  C=1.457e+11
<END EOS VARS>
```

C. SAND

```
format=00002

<OPTIONS>
  title="p-alpha sand    p-alpha eos using mieg eos as solid"
  eosType=p-al
<END OPTIONS>

<REFERENCE>
  rhoRef=0.13014274e+00
  eiRef=0.0
  cRef=313.282
<END REFERENCE>

<LIMITS>
  rhoMin=1.e-01
  eiMin=-1.e+09
  pMin=0.0
<END LIMITS>

<EOS VARS>
  gamma0=.96299999952
  S=1.8600000143
  rho0=0.13014274e+00
  ei0=0.0
  p0=4.036e+00
  c02=2.5197e+05
  ps=1.81297e+03
  pe=0.0
  alpha0=1.05195669
  ce2=4.31e+5
<END EOS VARS>
```

D. TNT

```
format=00002

<OPTIONS>
  title="tnt      ref: dobratz & crawford, ucid-52997 change 2, 1985, llnl"
  eosType=jwl
<END OPTIONS>

<REFERENCE>
  rhoRef=1.63
  eiRef=4.2945e+10
  cRef=.07e+5
<END REFERENCE>

<LIMITS>
  rhoMin=1.d-06
  eiMin=1.d+4
  pMin=0.
<END LIMITS>

<EOS VARS>
  A=3.712d+12
  B=.03231d+12
  R1=4.15d0
  R2=0.95d0
  omega=.30d0
  rho0=1.63
<END EOS VARS>
```

E. TNT UNBURNED MATERIAL

```
format=00002

<OPTIONS>
  title="tnt unburned material"
  eosType=burn
<END OPTIONS>

<REFERENCE>
  rhoRef=1.63
  eiRef=4.2945e+10
  cRef=5.77718e+5
<END REFERENCE>

<LIMITS>
  rhoMin=1.d-06
  eiMin=1.d+4
  pMin=0.
<END LIMITS>

<EOS VARS>
  p0=1.e+6
  rho0=1.63
  rhoCJ=2.227729
  eiCJ=6.022890e+10
  pCJ=2.099980e+11
  dCJ=6.929337e+05
  factor=.95
<END EOS VARS>
```

APPENDIX B. MATERIAL 45 (DTRA CONCRETE/ GEOLOGICAL MATERIAL)

A. MATERIAL TYPE 45 INPUT REQUIREMENTS

Columns		Quantity	Format
1-10	Card 3	Poisson's ratio ν	E10.0
11-20		Unconfined tensile strength, f_t	E10.0
21-30		Cohesion for max. failure surface, a_0	E10.0
31-40		Max. failure surface coefficient, a_1	E10.0
41-50		Max. failure surface coefficient, a_2	E10.0
51-60		Compressive damage scaling exponent, b_1	E10.0
61-70		Fractional dilatancy, ω	E10.0
71-80		Residual failure surface coefficient, a_{1f}	E10.0
1-10	Card 4	"Lambda stretch" factor, s: 0 for no stretch, 100 for stretching inversely with rate enhancement.	E10.0
11-20		Output selector for epx1, integer from 1 to 4, see text.	E10.0
21-30		Exponent *edrop* on η for post peak dilatancy decay (1 for linear drop, big for rapid drop)	E10.0
31-40		Critical value for the relative volume. When the relative volume of an element exceeds this value, the element is failed and removed from the calculation. Failed elements do not support any stresses.	E10.0
41-50		Not used	E10.0
51-60		Load curve giving rate sensitivity	E10.0
61-70		Not used	E10.0
71-80		Number of points in $\lambda - \eta$ relation (must be 13)	E10.0
1-10	Card 5	First tabulated value of damage function, λ_1 (=0)	E10.0
11-20		2nd tabulated value of damage function, λ_2	E10.0
21-30		3rd tabulated value of damage function, λ_3	E10.0
31-40		4th tabulated value of damage function, λ_4	E10.0
41-50		5th tabulated value of damage function, λ_5	E10.0
51-60		6th tabulated value of damage function, λ_6	E10.0

Columns		Quantity	Format
61-70		7th tabulated value of damage function, λ_7	E10.0
71-80		8th tabulated value of damage function, λ_8	E10.0
1-10	Card 6	9th tabulated value of damage function, λ_9	E10.0
11-20		10th tabulated value of damage function, λ_{10}	E10.0
21-30		11th tabulated value of damage function, λ_{11}	E10.0
31-40		12th tabulated value of damage function, λ_{12}	E10.0
41-50		13th tabulated value of damage function, λ_{13}	E10.0
51-60		Damage scaling coefficient for triaxial tension, b_3	E10.0
61-70		Cohesion for initial yield surface, a_{0_y}	E10.0
71-80		Initial yield surface coefficient, a_{1_y}	E10.0
1-10	Card 7	First tabulated value of scale factor, η_1	E10.0
11-20		2nd tabulated value of scale factor, η_2	E10.0
21-30		3rd tabulated value of scale factor, η_3	E10.0
31-40		4th tabulated value of scale factor, η_4	E10.0
41-50		5th tabulated value of scale factor, η_5	E10.0
51-60		6th tabulated value of scale factor, η_6	E10.0
61-70		7th tabulated value of scale factor, η_7	E10.0
71-80		8th tabulated value of scale factor, η_8	E10.0
1-10	Card 8	9th tabulated value of scale factor, η_9	E10.0
11-20		10th tabulated value of scale factor, η_{10}	E10.0
21-30		11th tabulated value of scale factor, η_{11}	E10.0
31-40		12th tabulated value of scale factor, η_{12}	E10.0
41-50		13th tabulated value of scale factor, η_{13}	E10.0
51-60		Tensile damage scaling exponent, b_2	E10.0
61-70		Residual failure surface coefficient, a_{2_f}	E10.0
71-80		Initial yield surface coefficient, a_{2_y}	E10.0

B. MATERIAL TYPE 45 INPUTS

```
*--I5---I5-------E10---I5---I5-------E10---I5-------E10-------E10---I5---I5XXXXI
    1   45168.559998   12    0    0.1000    0    1.5000    0.0600    0    0    0
*
 External No. :      1 ;   Mat.-Typ : 45
*
*------E10-------E10-------E10-------E10-------E10-------E10-------E10-------E10
  0.250000 96073.000 436500.00  0.446000  0.298700  1.000000       0.5    0.4417
         0  2.000000          0         0         0         0         0         0
         0         0         0         0         0         0         0         0
         0         0         0         0         0  1.150000 329400.00  0.625000
         0         0         0         0         0         0         0         0
         0         0         0         0         0  1.350000  0.349623  0.761131
*

*------E10-------E10-------E10-------E10-------E10-------E10-------E10-------E10
   0.0000000E+00   -1.460000E-03   -1.000000E-02   -4.000000E-02   -7.000000E-02
   -1.000000E+00   0.0000000E+00   0.0000000E+00   0.0000000E+00   0.0000000E+00
   0.0000000E+00   3.6250000E+03   1.5138000E+04   4.4350000E+04   8.0765000E+04
   1.0321100E+06   0.0000000E+00   0.0000000E+00   0.0200000E+00   0.0000000E+00
   0.0000000E+00   0.0000000E+00   0.0000000E+00   0.0000000E+00   0.0000000E+00
   0.0000000E+00   0.0000000E+00   0.0000000E+00   0.0000000E+00   0.0000000E+00
   2.4722500E+06   2.4722500E+06   4.4370000E+06   4.4370000E+06   4.4370000E+06
   4.4370000E+06   0.0000000E+00   0.0000000E+00   0.0000000E+00   0.0000000E+00
   0.0000000E+00   0.0000000E+00   0.0000000E+00
```

THIS PAGE INTENTIONALLY LEFT BLANK

LIST OF REFERENCES

[1] *Gemini*. 6th Ed. NSWD-IHD, Indian Head, MD, 2003.

[2] F. A. Costanzo, "Underwater explosion phenomena," in *Society for Experimental Mechanics*, Jacksonville, Florida, 2010, pp.1-4.

[3] H. Snay, "Hydrodynamics of underwater explosions," in *Naval Hydrodynamics Publication 515*, 1957,Washington, D.C., 1957, pp 325-352.

[4] V. Kedrinskii, "Rarefaction waves and bubbly cavitation in real liquid," presented at the Fourth International Symposium on Cavitation, Pasadena, CA, 2001.

[5] T. Moyer, "Full ship shock test modeling," unpublished.

[6] Beam bridges. (n.d.)World Association of Technology of Teachers. [Online]. Available: http://www.design-technology.org/beambridges.htm

[7] Bridge engineering (2016, Feb.). Brittanica. [Online]. Available: http://www.britannica.com/

[8] Beam bridge (2016, Feb.). Brittanica. [Online]. Available: http://www.britannica.com/

[9] M. Morrissey. (2000, Apr.). How bridges work. [Online]. Available: http://science.howstuffworks.com

[10] V. Alizadeh, "Rapid-Construction technique for bridge abutments using controlled low-strength materials," *Journal of Performance of Constructed Facilities*, vol. 28, no.1, pp. 149–156, Oct. 2012.

[11] W. D. Meyersohn, "Use of soil-cement piles for bridge," in *Contemporary Issues in Deep Foundations*, Denver, CO, 2007, pp. 170–179.

[12] T. M. Zayed, "Pile construction productivity assessment," *Journal of Construction Engineering and Management*, vol. 131, no. 6, pp. 705–714, Jun. 2005.

[13] L. F. Troyano, "Building the different elements of a bridge," in *Bridge Engineering: A Global Perspective*, Puerto, Madrid, Spain: Thomas Telford Publishing, 2003, pp. 253–265.

[14] Concrete pour for bridge pylons marks next step for the Mersey Gateway project (2015, Aug.) Mersey Gateway. [Online]. Available:

http://www.merseygateway.co.uk/

[15] Types of caissons (2013, Apr.). The Construction Civil. [Online]. Available: http://www.theconstructioncivil.org/

[16] M. Aggour, A. Hachichi and M. Mayer, “Nondestructive evaluation of timber bridge piles,” in *Proceedings of a Session a Structure Congress*, New Orleans, Lousiana, 1986, pp 82-95.

[17] Suspension bridge basi. (n.d.). Washington State Department of Trsnportation. [Online]. Available: http://www.wsdot.wa.gov/

[18] D. B. Gina Beim, “Transmission pier foundation,” in *Electrical Transmission and Substation Structures,* Branson, MO, 2015, pp. 452–463.

[19] M. Kostovos, “Effect of testing techiniques on the post-ultimate behavior of concrete in compression,” *Materiaux et Construction,* vol. 16, no. 91, pp. 3–12, 1983.

[20] J. V. Mier, *Concrete Fracture: A Multiscale Approach*, London, UK: CRC Press, 2013.

[21] A. Griffith, “The phenomena of rupture and flow in solids.,” *Philosophical Transactions of the Royal Society of London,* vol. 221, pp. 163–198, 1921.

[22] K. Newman, “Criteria for the behviour of plain concrete under complex states of stress,” in *Proceedings of international Conference on the Structure of Concrete and its Behaviour Under Load*, London, pp. 255-274, 1968.

[23] M. Kaplan, “Strains and stresses of concrete at initiation of cracking and near failure,” *Journal of the Americna Concrete Institute,* vol. 60, no. 7, pp. 853–879, 1963.

[24] P. Lowe, “Deformation and fracture of plain concrete,” *Magazine of Concrete Research,* vol. 30, no. 105, pp. 200–204, 1978.

[25] J. R. Eyre and H. S. Nasreddin, “Tension strain failure criterion for concrete,” *Magazine of Concrete Research,* vol. 65, no. 21, pp. 1303–1314, 2013.

[26] DYNA3D: A Nonlinear, Explicit, Three-DImensional Finite Element Code for Solid and Structural Mechanics, 13th ed., LLNL. , Livermore, CA, 2013.

[27] Gemini: The DYSMAS Eulerian Solver: User's Manual, NSWC-IHD, Indian Head, MD, 2010.

[28] A.B. Wardlaw, "The GEMINI Euler solver for the coupled situation of underwater explosions," NSWC Indian Head, Indian Head, 2003.

[29] LS-DYNA Theoretical Maual, Livermore Software Technology Co., Livermore, CA, 1998.

[30] A. P. Walters, "Investigation of an explicitly modeled solid ocean floor on a shallow water UNDEX event," M.S. thesis, Dept. Mech. Eng., Naval Postgraduate School, Monterey, CA, 2011.

[31] R. Buxton, "The effects of porous sea bottoms on the propogation of underwater shock waves using the P-Alpha equation of etate," M.S. thesis, Dept, Mech. Eng., The Pennsylvania State University, The Graduate School, State College, PA, 2009.

[32] "P-alpha (Mat#5, Code =P-Al)," *DYSMAS User's Manual*, Office of Naval Research, 2014, ch. 7, sec. 5, pp. 1467–147.

[33] "Tillotson (Mat#8, Code=Till)," *Dysmas User's Manual*, Office of Naval Research, 2014, ch. 7, sec. 8, p. 151.

[34] "Gamma-Law (Mat #1, Code=g_law)," *Dysmas User's Manual*, Office of Naval Research, 2014, ch. 7, sec. 1, p. 136.

[35] S. M. Arbogast, "The influence of shock-inudced air bubble collapse resulting from underwater exposive events," M.S. thesis, Dept. Mech. Eng., Naval Postgraduate School, Monterey, CA, 2012.

[36] "Tait for Unburned Explosive (Mat#10, Code=Burn)," *DYSMAS User's Manual*, Office of Naval Research, 2014, ch. 7, sec. 3, pp. 156–157.

[37] "JWL(Mat #2, Code=JWL)," *DYSMAS User's Manual*, Office of Naval Research, 2014, ch. 7, sec. 2, pp. 137–140.

[38] E. K. C. Noble, "Concrete model description and summary of benchmark studies for blast effect simulations," LLNL, Livermore, CA, Jul. 2005.

THIS PAGE INTENTIONALLY LEFT BLANK

INITIAL DISTRIBUTION LIST

1. Defense Technical Information Center
   Ft. Belvoir, Virginia

2. Dudley Knox Library
   Naval Postgraduate School
   Monterey, California